The Quasicontinuum Method: Overview, applications and current directions

RONALD E. MILLER[a] and E. B. TADMOR[b]

[a]*Department of Mechanical and Aerospace Engineering, Carleton University, Ottawa, ON, K1S 5B6, Canada*
[b]*Department of Mechanical Engineering, Technion – Israel Institute of Technology, Haifa, 32000, Israel*

Abstract. The Quasicontinuum (QC) Method, originally conceived and developed by Tadmor, Ortiz and Phillips [1] in 1996, has since seen a great deal of development and application by a number of researchers. The idea of the method is a relatively simple one. With the goal of modeling an atomistic system without explicitly treating every atom in the problem, the QC provides a framework whereby degrees of freedom are judiciously eliminated and force/energy calculations are expedited. This is combined with adaptive model refinement to ensure that full atomistic detail is retained in regions of the problem where it is required while continuum assumptions reduce the computational demand elsewhere. This article provides a review of the method, from its original motivations and formulation to recent improvements and developments. A summary of the important mechanics of materials results that have been obtained using the QC approach is presented. Finally, several related modeling techniques from the literature are briefly discussed. As an accompaniment to this paper, a website designed to serve as a clearinghouse for information on the QC method has been established at www.qcmethod.com. The site includes information on QC research, links to researchers, downloadable QC code and documentation.

1. Introduction

The traditional analytical and computational framework in mechanics has been the continuum. Materials are assumed to be comprised of an infinitely divisible continuous medium, imbued with a constitutive behaviour that remains unchanged regardless of how small the structure of interest may be. By careful fitting of the mathematical form of the constitutive laws to experimental observations, the behaviour of real materials is introduced into the continuum framework, and structures can then be analyzed through the solution of boundary value problems.

However, in recent years there has been a significant shift in the focus of mechanics of materials. The advent of powerful microscopy tools, the development of micro- and nano- scale technologies such as computer chips and micro-electromechanical systems (MEMS), and the development of computational tools predicated on the fundamental interactions between the atoms in a material have led the science of mechanics to focus increasingly on the *nano-scale*.

The shift in focus to the nano-scale quickly revealed the failings of continuum mechanics in this new paradigm. Suddenly, the fact that materials are ultimately comprised of discrete particles became an essential feature that had to be included in the material description. For example, detailed understanding of the behaviour of grain boundaries requires that the atomic structure of the boundary be correctly modeled. Also, atomic scale competition between dislocation nucleation and brittle cleavage at a crack tip depends on the details of bond breaking and rearrangement in the tip region. As a final example, the behaviour of very small structures like

those found in MEMS devices, particularly their failure through fracture and fatigue processes, can often be affected by surface properties that are negligible in larger systems.

At the same time, however, it must be recognized that it is neither practical nor necessary to abandon continuum mechanics altogether. In order to adopt a purely atomistic picture of a material, in which every atom must be tracked during the course of the material's deformation process, one must limit the scale of the problem to systems that are tiny even in comparison to modern micro- and nano-scale engineered systems. Consider that the current benchmark for large-scale fully atomistic simulations is on the order of 10^9 atoms, using massively paralleled computer facilities with hundreds or thousands of CPUs. This represents 1/10,000 of the number of atoms in a typical grain of aluminum, and 1/1,000,000 of the atoms in a typical MEMS device. Further, it is apparent that with such a large number of atoms, substantial regions of a problem of interest are essentially behaving *like a continuum*. Clearly, while fully atomistic calculations are essential to our understanding of the basic "unit" mechanisms of deformation, they will never replace continuum models altogether.

The goal for many researchers, then, has been to develop techniques that retain a largely continuum mechanics framework, but impart on that framework enough atomistic information to be relevant to modeling a problem of interest. In many examples, this means that certain, relatively small, fractions of a problem require full atomistic detail while the rest can be modeled using the assumptions of continuum mechanics. As an example, consider the fracture simulation shown in Fig. 1. This is a fully atomistic simulation involving 1.2×10^6 atoms, divided into two fcc grains separated by a tilt boundary. One of the grains contains a crack, which when loaded quickly nucleates an avalanche of dislocation loops that ultimately interact with the grain boundary. In the figure, the vast majority of the atoms are not shown, so that the important details of the simulation can be visualized. It is precisely these omitted atoms, occupying most of the simulation volume, that are experiencing a deformation which is essentially that of a nonlinear elastic continuum. It seems that it should be possible to simultaneously treat the regions around the crack, grain boundary and dislocation cores as atomistic, while still using the efficiencies of continuum mechanics for the bulk of the crystal and the application of the boundary conditions.

The quasicontinuum method (QC) has been developed with such a goal in mind. The QC philosophy is to consider the atomistic description as the "exact" model of material behaviour, but at the same time acknowledge that the sheer number of atoms make most problems intractable in a fully atomistic framework. Then, the QC uses continuum assumptions to reduce the degrees of freedom and computational demand without losing atomistic detail in regions where it is required.

The purpose of this article is to review the development of the QC, from its original implementation through recent extensions and modifications. A variety of applications will be discussed to highlight key materials problems that have been addressed with the method. We note that in the past, other reviews have been written which discuss at some length various aspects of the QC. While the present review will, of course, provide a more up-to-date perspective and reflect the most advances, the reader may also be interested in the reviews by Ortiz *et al.* [3], Ortiz and Phillips [4], and Rodney [5].

As a final matter of interest, we note that many other researchers have developed methods independently that are in many ways similar to the QC. In some instances, these may be completely different approaches with the same underlying philosophy of merging atomistics and continuum mechanics, while in others the work may be an off-shoot of the QC or a development inspired by some aspect of the QC approach. Although it is outside the scope
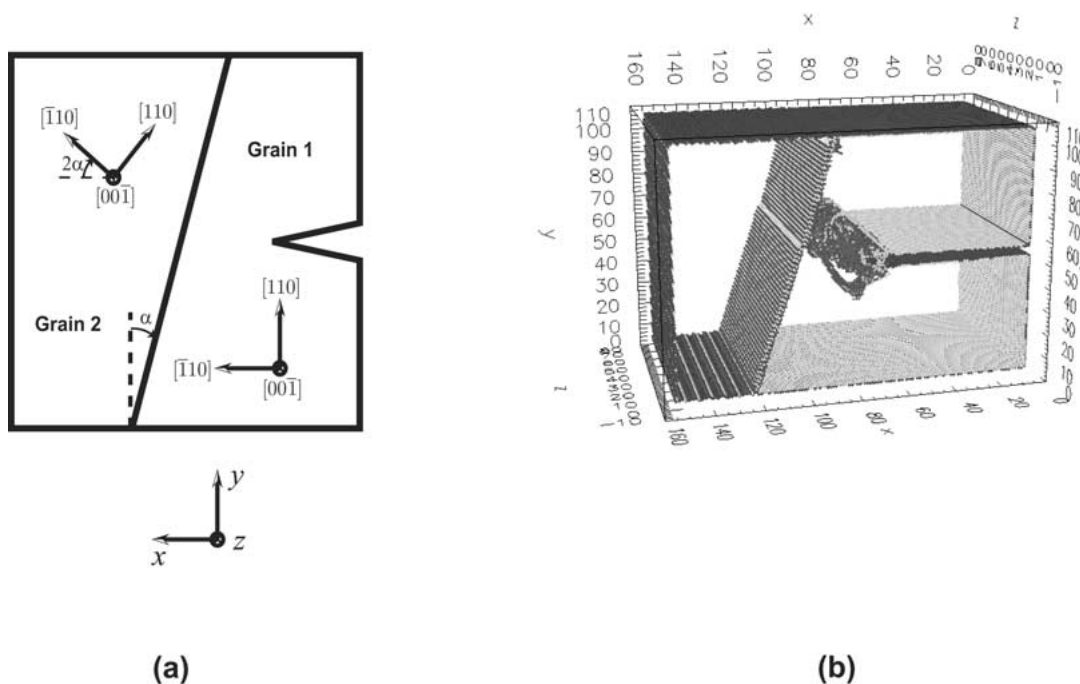
(a) **(b)**

Figure 1. A fully atomistic simulation of a crack near a grain boundary is schematically shown in (a). In (b), most of the 1.2×10^6 atoms in the simulation are not shown to reveal the important atomistic details of the dislocation loops emitting from the crack and impinging on the grain boundary (reproduced from [2], with permission, published by Taylor and Francis, www.tandf.co.uk).

of this paper to discuss all of them in detail, we will provide a brief literature review of these techniques.

The organization of the remaining sections is as follows. First, a brief review of atomistic methods is provided in Section 2. This is considered relevant since the atomistic model is viewed as the benchmark "exact" description of material behaviour that the QC aims to reproduce with reduced computational overhead. In Sections 3 and 4, the current state of the QC is presented, based on the cumulative work presented in references [1, 6, 7, 8, 9]. In Section 5, a number of applications are presented. Section 6 discusses the current directions being taken with the QC. Finally, we review related simulation techniques in Section 7.

As noted in the abstract, as an accompaniment to this paper, a website designed to serve as a clearinghouse for information on the QC method has been established at www.qcmethod.com. The site includes information on QC research, links to researchers, downloadable QC code and documentation. The downloadable code is freely available and corresponds to the full QC implementation discussed in Section 3.4.

2. Atomistic modeling

In the QC, the point-of-view which is adopted is that there is an underlying atomistic model of the material which is the "correct" description of the material behaviour. This could, in principle, be a quantum-mechanically based description such as density functional theory (DFT), but in practice the focus has been primarily on atomistic models based on semi-empirical interatomic potentials. A review of such methods can be found, for example, in [10]. Here,

we present just the features of such models which are essential for our discussion. For now we focus on *lattice statics* solutions, *i.e.* we are looking for equilibrium atomic configurations for a given model geometry and externally imposed forces or displacements, because most applications of the QC have used a static implementation. In Section 6, we will discuss recent work to extend QC to finite temperature, dynamic simulations.

We assume that there is some reference configuration of N atomic nuclei, described by a lattice. Thus, the reference position of the ith atom in the model X_i is found from an integer combination of lattice vectors and a reference (origin) atom position, X_0

$$X_i = X_0 + l_i A_1 + m_i A_2 + n_i A_3, \tag{1}$$

where (l_i, m_i, n_i) are integers, A_j is the jth Bravais lattice vector.

The deformed position of the ith atom x_i, is then found from a unique displacement vector u_i for each,

$$x_i = X_i + u_i. \tag{2}$$

The displacements u_i, while only having physical meaning on the atomic sites, can be treated as a continuous field $u(X)$ throughout the body with the property that $u(X_i) \equiv u_i$. This approach, while not the conventional one in atomistic models, is useful in effecting the connection to continuum mechanics. Note that for brevity we will often refer to the field u to represent the set of all atomic displacements $\{u_1, u_2, \ldots u_N\}$ where N is the number of atoms in the body.

In standard lattice statics approaches using semi-empirical potentials, there is a well defined total energy function E^{tot} that is determined from the relative positions of all the atoms in the problem. In many semi-empirical models, this energy can be written as a sum over the energy of each atom individually, *i.e.*,

$$E^{tot} = \sum_{i=1}^{N} E_i(u), \tag{3}$$

where E_i is the site energy of atom i, which depends on the displacements u through the relative positions of all the atoms in the deformed configuration. For example, within the Embedded Atom Method (EAM) [11, 12] atomistic model, this site energy is given by

$$E_i = F_i(\bar{\rho}_i) + E_i^{(2)}, \tag{4}$$

where

$$E_i^{(2)} = \frac{1}{2} \sum_{j \neq i} V_{ij}^{(2)}(r_{ij}), \tag{5}$$

F_i can be interpreted as an electron-density dependent embedding energy, $V_{ij}^{(2)}$ is a pair potential between atom i and its neighbor j and $r_{ij} = \sqrt{(x_i - x_j) \cdot (x_i - x_j)}$ is the interatomic distance. The spherically averaged electron density at the position of atom i, $\bar{\rho}_i$, is the superposition of density contributions from each of the neighbors, ρ_j:

$$\bar{\rho}_i = \sum_{j \neq i} \rho_j(r_{ij}). \tag{6}$$

The QC has also been formulated in terms of 3-body interaction potentials of the Stillinger-Weber (SW) type [13]. The main difference between the EAM and SW type of atomistic law is that instead of the embedding energy, F_i, of the EAM, SW includes a term involving three-body interactions to account for the directional bonding in covalent silicon. The energy of an atom i in the SW formulation is then

$$E_i = E_i^{(2)} + E_i^{(3)}, \tag{7}$$

$E_i^{(2)}$ is as described in eqn (5) (although the functional form of $V_{ij}^{(2)}$ is different from that of the EAM), and $E_i^{(3)}$ is the three-body contribution, which is written

$$E_i^{(3)} = \frac{1}{6} \sum_{j \neq i} \sum_{k \neq (i,j)} V_{ijk}^{(3)}(\boldsymbol{r}_{ij}, \boldsymbol{r}_{ik}), \tag{8}$$

where $V_{ijk}^{(3)}$ is the three-body potential and $\boldsymbol{r}_{ij}$ is the vector from atom i to neighbor atom j:

$$\boldsymbol{r}_{ij} = \boldsymbol{x}_j - \boldsymbol{x}_i. \tag{9}$$

In both the EAM and the SW framework, the exact details of the functions ρ_j, F_i, $V_{ij}^{(2)}$ and $V_{ijk}^{(3)}$ are defined to produce a best-fit to various properties of a given material, and thus can be used to describe a wide range of metallic and semi-conducting crystals.

In addition to the potential energy of the atoms, there may be energy due to external loads applied to atoms. Thus, the total potential energy of the system (atoms plus external loads) can be written as

$$\Phi(\boldsymbol{u}) = E^{tot}(\boldsymbol{u}) - \sum_{i=1}^{N} \boldsymbol{f}_i \boldsymbol{u}_i, \tag{10}$$

where $-\boldsymbol{f}_i \boldsymbol{u}_i$ is the potential energy of the applied load $\boldsymbol{f}_i$ on atom i. In lattice statics, we seek the displacements $\boldsymbol{u}$ such that this potential energy is minimized.

3. The QC method

The goal of the static QC method is to find the atomic displacements that minimize eqn. (10) by approximating the total energy of eqn. (3) such that:

(1) the number of degrees of freedom is substantially reduced from $3N$, but the full atomistic description is retained in certain "critical" regions.

(2) the computation of the energy in eqn. (3) is accurately approximated without the need to explicitly compute the site energy of all the atoms.

(3) the fully atomistic, critical regions can evolve with the deformation, during the simulation.

In this section, the details of how the QC achieves each of these goals are presented.

3.1. REMOVING DEGREES OF FREEDOM

A key measure of a displacement field is the deformation gradient $\boldsymbol{F}$. A body deforms from reference state X to deformed state $\boldsymbol{x} = X + \boldsymbol{u}(X)$, from which we define

$$\boldsymbol{F}(X) \equiv \frac{\partial \boldsymbol{x}}{\partial X} = \boldsymbol{I} + \frac{\partial \boldsymbol{u}}{\partial X}, \tag{11}$$
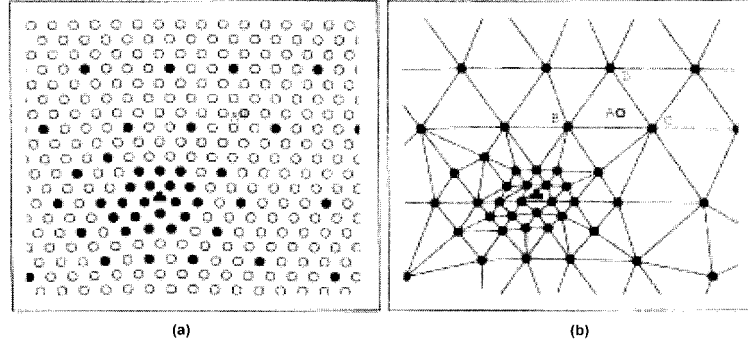
Figure 2. Selection of repatoms from all the atoms near a dislocation core are shown in (a), which are then meshed by linear triangular elements in (b). The density of the repatoms varies according to the severity of the variation in the deformation gradient.

where I is the identity tensor. If the deformation gradient changes gradually on the atomic scale, then it is not necessary to explicitly track the displacement of every atom in the region. Instead, the displacements of a small fraction of the atoms (called representative atoms or "repatoms") can be treated explicitly, with the displacements of the remaining atoms approximately found through interpolation. In this way, the degrees of freedom are reduced to only those of the repatoms.

The QC incorporates such a scheme by recourse to the interpolation functions of the finite element method (FEM) (see, for example, [14]). Fig. 2 illustrates the approach in two-dimensions in the vicinity of a dislocation core. The filled atoms are the selected repatoms, which are meshed by a space-filling set of linear triangular finite elements. Any atom not chosen as a repatom, like the one labeled "A", is subsequently constrained to move according to the interpolated displacements of the element in which is resides. The density of repatoms is chosen to vary in space according to the needs of the problem of interest. In regions where full atomistic detail is required, all atoms are chosen as repatoms, with correspondingly fewer in regions of more slowly varying deformation gradient. This is illustrated in Fig. 2, where all the atoms around the dislocation core are chosen as repatoms. Further away, where the crystal experiences only the linear elastic strains due to the dislocation, the density of repatoms is reduced.

This first approximation of the QC then, it to replace the energy E^{tot} by $E^{tot,h}$:

$$E^{tot,h} = \sum_{i=1}^{N} E_i(\boldsymbol{u}^h). \tag{12}$$

In this equation the atomic displacements are now found through the interpolation functions and take the form

$$\boldsymbol{u}^h = \sum_{\alpha=1}^{N_{rep}} S_\alpha \boldsymbol{u}_\alpha, \tag{13}$$

where S_α is the interpolation function associated with repatom α, and N_{rep} is the number of repatoms, $N_{rep} \ll N$. Note that the formal summation over the shape functions in eqn. (13) is in practice much simpler due to the compact support of the finite element shape functions. Specifically, shape functions are identically zero in every element not immediately adjacent

to a specific repatom. Referring back to Fig. 2, this means that the displacement of atom A is determined entirely from the sum over the three repatoms B, C and D defining the element containing A:

$$u^h(X_A) = S_B(X_A)u_B + S_C(X_A)u_C + S_D(X_A)u_D. \tag{14}$$

Introducing this kinematic constraint on most of the atoms in the body will achieve the goal of reducing the number of degrees of freedom in the problem, but notice that for the purpose of energy minimization we must still compute the energy and forces on the degrees of freedom by explicitly visiting every atom – not just the repatoms – and building its neighbor environment from the interpolated displacement fields. In the next two sections, we discuss how these calculations are approximated and made computationally tractable.

3.2. EFFICIENT ENERGY/FORCE CALCULATIONS: THE LOCAL QC

In addition to the degree of freedom reduction described in the previous section, the QC requires an efficient means of computing the energy and forces without the need to visit every atom in the problem as implied by eqn. (12). The first way to accomplish this is by recourse to the so-called Cauchy-Born (CB) rule (see [15] and references therein), resulting in what is referred to as the *local* formulation of the QC.

The use of linear shape functions to interpolate the displacement field means that within each element, the deformation gradient will be uniform. The Cauchy-Born rule assumes that a uniform deformation gradient at the macro-scale can be mapped directly to the same uniform deformation on the micro-scale. For crystalline solids with a simple lattice structure, this means that every atom in a region subject to a uniform deformation gradient will be energetically equivalent. Thus, the energy within an element can be estimated by computing the energy of *one* atom in the deformed state and multiplying by the number of atoms in the element. In practice, the calculation of the CB energy is done separately from the model in a "black box", where for a given deformation gradient F, a unit cell with periodic boundary conditions is deformed appropriately and its energy is computed. The strain energy density in the element is then given by

$$\mathcal{E}(F) = \frac{E_0(F)}{\Omega_0}, \tag{15}$$

where Ω_0 is the unit cell volume (in the reference configuration) and E_0 is the energy of the unit cell when its lattice vectors are distorted according to F,

$$a_i = FA_i. \tag{16}$$

Here a_i are the lattice vectors in the current configuration. Now the total energy of an element is simply this energy density times the element volume, and the total energy of the problem is simply the sum of element energies:

$$E^{tot,h} \approx E^{tot,h'} = \sum_{e=1}^{N_{element}} \Omega_e \mathcal{E}(F_e), \tag{17}$$

where Ω_e is the volume of element e. The important computational saving made here is that a sum over all the *atoms* in the body has been replaced by a sum over all the *elements*, each one requiring an explicit energy calculation for only one atom. Since the number of
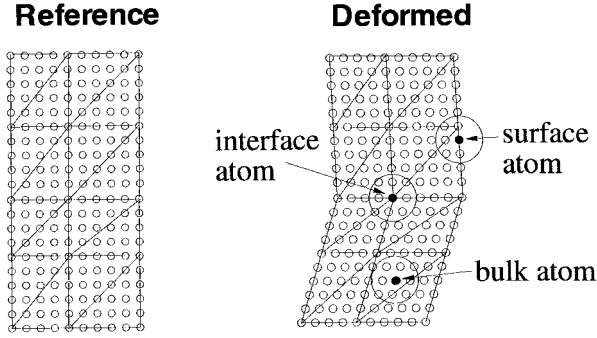
Reference   **Deformed**

Figure 3. On the left, the reference configuration of a square lattice meshed by triangular elements. On the right, the deformed mesh shows a bulk atom, for which the CB rule is exactly correct, and two other atoms for which the CB rule will give the wrong energy due to its inability to describe surfaces or changes in the deformation gradient.

elements is typically several orders of magnitude smaller than the total number of atoms, the computational savings is substantial. The number of elements scales linearly with the number of repatoms, and so the local QC scales as $\mathcal{O}(N_{rep})$.

Note, however, that even in the case where the deformation is uniform within each element, the local prescription for the energy in the element is only approximate. This is because in the constrained displacement field $\boldsymbol{u}^h$, the deformation gradient varies from one element to the next. At element boundaries and free surfaces, atoms can have energies that differ significantly from that of an atom in a bulk, uniformly deformed lattice. Fig. 3 illustrates this schematically for an initially square lattice deformed according to two different deformation gradients in two neighboring regions. The energy of the atom labeled as a "bulk atom" can be accurately computed from the CB rule; its neighbor environment is uniform even though some of its neighbors occupy other elements. However, the "interface atom" and "surface atom" are not accurately described by the CB rule, which assume that these atoms see uniformly deformed bulk environments.

In situations where the deformation is varying slowly from one element to the next and where surface energetics are not important, the local approximation is a reasonably good one. Using the CB rule as in eqn. (15), the QC can be thought of as a purely continuum formulation, but with a constitutive law that is based on atomistics rather than on an assumed phenomenological form. The CB constitutive law automatically ensures that the correct anisotropic crystal elasticity response will be recovered for small deformations. It is non-linear elastic (again as dictated by the underlying atomistic potentials) for intermediate strains and includes lattice invariance for large deformations. For example, a shear deformation that corresponds to the twinning of the lattice will lead to a rotated crystal structure with zero strain energy density.

An advantage of the local QC formulation is that it allows the use of quantum mechanical atomistic models that cannot be written as a sum over individual atom energies such as tight binding (TB) and DFT. In these models only the total energy of a collection of atoms can be obtained. However, for a lattice undergoing a uniform deformation it is possible to compute the energy density $\mathcal{E}(\boldsymbol{F})$ from a single unit cell with periodic boundary conditions. Incorporation of quantum mechanical information into the atomic model generally ensures that the description is more transferable, *i.e.*, it provides a better description of the energy of atomic configurations away from the reference structure to which empirical potentials are fitted. This allows truly first-principles simulations of some macroscopic processes such as phase transformations. See sections 5.1 and 5.5 for examples of such applications.

3.3. MORE ACCURATE CALCULATIONS: THE NONLOCAL QC

The local QC formulation successfully imbues the continuum FEM framework with atomistic properties such as nonlinearity, crystal symmetry and lattice invariance. The latter property means that dislocations may exist in the local QC. However, the core structure and energy of these dislocations will only be coarsely represented due to the uniform deformation constraint. The same is true for other defects such as surfaces and interfaces, where the deformation of the crystal is non-uniform over distances shorter than the cut-off radius of the interatomic potentials. For example, to correctly account for the energy of the interface shown in Fig. (3), the non-uniform environment of the atoms along the interface must be correctly accounted for. While the local QC can support deformations (such as twinning) which may lead to microstructures containing such interfaces, it will not account for the energy cost of the interface itself.

In order to correctly capture these details, the QC must be made nonlocal. The energy of eqn. (12), which in the local QC was approximated by eqn. (17), must instead be approximated in a way that is sensitive to non-uniform deformation and free surfaces, especially in the limit where full atomistic detail is required.

The nonlocal QC has been formulated in two ways, which we define as the *energy-based* formulation and the *force-based* formulation. Both start from the energy of eqn. (12), with the goal of finding equilibrium configurations of the atoms. In practice, this involves computing the total energy and the forces (derivatives of the total energy) on each repatom, and then driving the system to the energy minimizing (zero force) configuration. The difficulty, however, is to determine this equilibrium configuration without the need to explicitly compute energy and force contributions from every atom in the problem as eqn. (12) currently dictates.

In the energy-based formulation, the ansatz is made that one can accurately approximate the energy by an expression obtained by explicitly computing only the energy of the repatoms ($N_{rep} \ll N$). Specifically, the new approximate energy takes the form

$$E^{tot,h} \approx E^{tot,h'} = \sum_{\alpha=1}^{N_{rep}} n_\alpha E_\alpha(\boldsymbol{u}_h). \tag{18}$$

The important difference here is that the sum on *all* the atoms in the problem has been replaced with a sum on *only* the repatoms. The function n_α is a weight function for repatom α, which will be high for repatoms in regions of low repatom density and vice versa. For consistency, the weight functions must be chosen so that

$$\sum_{\alpha=1}^{N_{rep}} n_\alpha = N, \tag{19}$$

which further implies (through the consideration of a special case where every atom in a problem is made a repatom) that in atomically refined regions, all $n_\alpha = 1$. From eqn. (19), the weight functions can be physically interpreted as the number of atoms represented by each repatom α.

The energy of each repatom, E_α, is then computed from the deformed neighbor environment dictated from the current interpolated displacements in the elements. For example, the energy of the repatom identified as an "interface atom" in Fig. 3 requires that the neighbor environment be generated by displacing each neighbor according to the element in which it

resides. Thus, the energy of each repatom is exactly as it should be under the displacement field u^h, with the energy of all the other atoms in the problem being approximated through the weight function n_α. From this starting point, the forces on all the repatoms can be obtained as the derivatives of eqn. (18) with respect to the repatom positions and energy minimization can proceed.

In the *force-based* QC formulation, the starting point is to recognize that energy minimization physically corresponds to solving for the configuration for which the force on each degree of freedom is zero. Equilibrium can be sought be working directly from an approximate expression for the forces, rather than from the explicit differentiation of an energy functional. This formulation, advocated in [9], starts from the derivatives of eqn. (12) with respect to each repatom displacement:

$$f_\alpha \equiv \frac{\partial E^{tot,h}}{\partial u_\alpha} = \sum_{i=1}^{N} \frac{\partial E_i(u^h)}{\partial u^h} \frac{\partial u^h}{\partial u_\alpha}, \tag{20}$$

where we recall that the notation u^h implies the interpolated displacement field and u_α the displacement of a specific repatom. Because of eqn. (13),

$$\frac{\partial u^h}{\partial u_\alpha} = S_\alpha, \tag{21}$$

and so the force expression becomes

$$f_\alpha = \sum_{i=1}^{N} \frac{\partial E_i(u^h)}{\partial u^h(X_i)} S_\alpha(X_i). \tag{22}$$

This summation can be suitably approximated by visiting only a small subset of all the atoms in the problem. Specifically, a *cluster* of sampling points is defined around each repatom as shown in Fig. 4. In regions of high repatom density, the clusters are suitably shrunk so that there is no overlap between neighboring clusters. The forces are then approximated as

$$f_\alpha \approx \sum_{\beta}^{N_{rep}} n_\beta \left[\sum_{c \in \mathcal{C}_\beta} g_c S_\alpha(X_c) \right]. \tag{23}$$

where $\mathcal{C}_\beta$ refers to the set of atoms in the cluster around repatom β and

$$g_c = \frac{\partial E^{tot,h}}{\partial u_c^h}, \tag{24}$$

is the atomic-level force experienced by cluster atom c in displacement field u^h. The optimal cluster size is a trade-off between computational efficiency and error in the approximation, but was found by Knap and Ortiz [9] to be on the order of first or second neighbor shells.

The fully non-local description, as described here, has certain disadvantages, the main one being the significant increase in computational cost as compared with the local approach. Each energy or force evaluation requires the mapping of a cluster of atoms and their neighbors to their deformed configuration at every repatom, followed by the necessary interatomic potential evaluations necessary to compute the energy or forces for the cluster. This is more than is required in the local calculation, but can be made reasonably efficient with careful
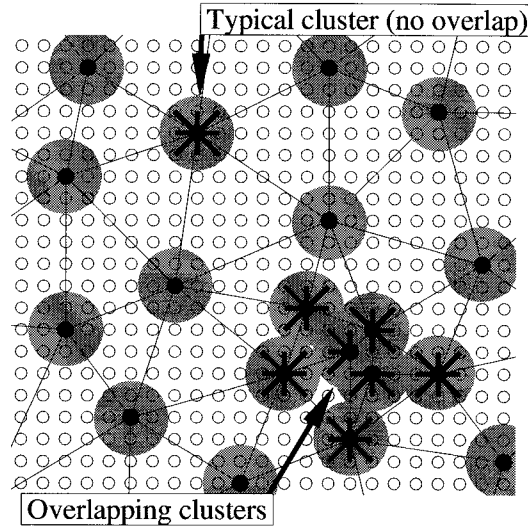
Figure 4. Schematic of cluster selection for the force-based non-local QC. Typical clusters in this example, in regions of no overlap, contain 9 atoms as indicated by the gray region and heavy lines joining the cluster atoms to the repatom. In regions where the clusters overlap, cluster size is reduced so that no atom is in more than one cluster. Degeneracies (where a cluster atom is equidistant to two repatoms) are resolved randomly.

bookkeeping and look-up tables [9]. Despite the increase demand per repatom, the nonlocal formulation still scales as $\mathcal{O}(N_{rep})$ since the cluster size per repatom is constant.

While the local QC suffered from an inability to resolve *any* energy of free surfaces or interfaces, the nonlocal QC suffers from a significant overestimate of surface effects. Consider a repatom at the corner of a cubic specimen. The cluster for this repatom will be a high energy cluster due to the three free surfaces it will see. At the same time, if this repatom has a large weight n_α because it represents a large volume of material, the resulting energy will be as though that entire volume of material is located in the vicinity of a corner. The result is a significant overestimate of the energetic importance of the corner and therefore spurious relaxations of this repatom.

The main advantage of the nonlocal QC, both energy and force-based, is that when it is refined down to the atomic scale, it reduces exactly to lattice statics, correctly capturing details of dislocation cores, stacking faults and grain boundaries.

3.4. COUPLED LOCAL/NONLOCAL QC

Recognizing that the nonlocal QC is exactly correct in regions where atomic scale accuracy is needed, while the local QC has the advantage of computational efficiency in regions where the deformation is changing relatively slowly on the atomic scale and the convenience of direct application of continuum boundary conditions, it seems desirable to have the ability to use both formulations in a single simulation. Such a formulation has been developed by combining the local QC and the energy-based formulation of the nonlocal QC as presented above.[4]

We return to the energy of eqn. (12). As in the energy-based nonlocal QC, we again use the ansatz that this energy can be approximated by computing only the energy of the repatoms, but this time assume that we can treat each repatom as being either *local* or *nonlocal* depending
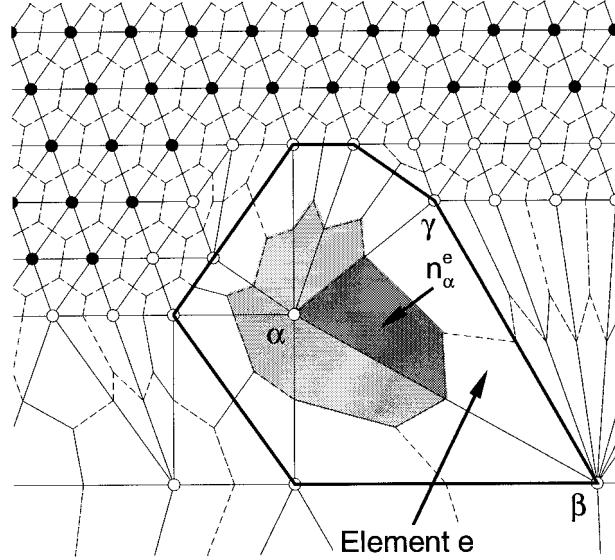
Figure 5. A QC mesh showning local and nonlocal repatoms and associated meshing (solid lines) and tesselation (dashed lines). Highlighted is local repatom α and element e (defined by repatoms α, β and γ) which is connected to it. The total number of atoms represented by repatom α is n_α. Of those n_α^e are found in element e.

on its deformation environment. Thus, the repatoms are divided into N_{loc} local repatoms and N_{nl} nonlocal repatoms ($N_{loc} + N_{nl} = N_{rep}$). The energy expression is then approximated as

$$E^{tot,h} \approx \sum_{\alpha=1}^{N_{nl}} n_\alpha E_\alpha(\boldsymbol{u}_h) + \sum_{\alpha=1}^{N_{loc}} n_\alpha E_\alpha(\boldsymbol{u}_h). \tag{25}$$

The weight n_α for each repatom (local or nonlocal) is determined from a tessellation that divides the body into cells around each repatom. One physically sensible tessellation is Voronoi cells [16], but an approximate Voronoi diagram can be used instead due to the high computational overhead of the Voronoi construction. In practice, the coupled QC formulation makes use of a simple tessellation based on the existing mesh, partitioning each element equally between each of its nodes. An example of such a tesselation is shown in Fig. 5. In this figure the finite elements are drawn with solid lines and the corresponding tesselation is dashed. The volume of the tessellation cell for a given repatom, divided by the volume of a single atom (the Wigner-Seitz volume) provides n_α for the repatom. In the figure, local repatom α is highlighted. The voronoi cell surrounding it appears shaded. The dark line further out marks the edges of the elements surrounding the node. The voronoi cell of repatom α contains a total of n_α atoms. Of these atoms, n_α^e reside in element e (as indicated by the dark shading in the figure). The weighted energy contribution of repatom α is then found by applying the CB rule within each element adjacent to α such that

$$n_\alpha E_\alpha = \sum_{e=1}^{M} n_\alpha^e \Omega_0 \mathcal{E}(\boldsymbol{F}_e), \quad n_\alpha = \sum_{e=1}^{M} n_\alpha^e, \tag{26}$$

where $\mathcal{E}(\boldsymbol{F}_e)$ is the energy density in element e by the CB rule, Ω_0 is the Wigner-Seitz volume of a single atom and M is the number of elements adjacent to α.

Note that this description of the local repatoms is exactly equivalent to the element-by-element summation of the local QC in 3.2. In a mesh containing only local repatoms, the two formulations are the same, but the summations have been rearranged from one over elements in eqn. (17) to one over the repatoms here.

3.4.1. *The Local/Nonlocal Criterion*

When making use of the mixed formulation described in eqn.v(25), it now becomes necessary to decide whether a given repatom should be local or nonlocal. This is achieved automatically in the QC using a *nonlocality criterion*. Note that simply having a large deformation in a region does not in itself require a nonlocal repatom, as the CB rule of the local formulation will exactly describe the energy of any *uniform* deformation, regardless of the severity. The key feature that should trigger a nonlocal treatment of a repatom is a significant *variation* in the deformation gradient on the atomic scale in the repatom's proximity. Thus, the nonlocality criterion in implemented as follows. A cutoff is defined r_{nl}, empirically chosen to be between two and three times the cutoff radius of the interatomic potentials. The deformation gradients in every element within this cutoff of a given representative atom are compared, by looking at the differences between their eigenvalues. The criterion is then:

$$\max_{a,b;k} |\lambda_k^a - \lambda_k^b| < \epsilon, \tag{27}$$

where λ_k^a is the kth eigenvalue of the right stretch tensor $\boldsymbol{U}_a = \sqrt{\boldsymbol{F}_a^T \boldsymbol{F}_a}$ in element a, $k = 1 \ldots 3$, and the indices a and b run over all elements within r_{nl} of a given repatom. The repatom will be made local if this inequality is satisfied, and non-local otherwise. In practice, the tolerance ϵ is determined empirically. A value of 0.1 has been used in a number of tests and found to give reasonable results.

In practice, the effect of this criterion is clusters of nonlocal atoms in regions of rapidly varying deformation. In the mixed QC, a further restriction is imposed on nonlocal repatoms, in that they must have a weight of $n_\alpha = 1$. This ensures that nonlocal regions are also regions of full atomistic refinement, which avoids the problem (described at the end of section 3.3) of highly energetic nonlocal repatoms overestimating the energy of neighboring unrepresented atoms. The result of this is that there are well defined interfaces between local and nonlocal regions. In the next section, these interfaces are examined in some detail.

3.4.2. *Effects of the Nonlocal/Local Interface*

The fact that the nonlocal repatoms tend to cluster into atomistically refined regions surrounded by local regions leads to nonlocal/local interfaces in the mixed QC. One such interface is illustrated in Fig. 6, to highlight some of the important details. In the figure, nonlocal repatoms are shown filled, local atoms are shown open. Material (atoms) contained in the elements joining only *local* repatoms, such as element A, contributes all of its energy to the model, as all segments of these elements lie in the tessellation cells of local repatoms. On the other hand, there is no energy "in" the elements joining only *nonlocal repatoms* like element B, since the CB rule is not used in these nonlocal regions. Finally, elements joining a mixture of local and nonlocal repatoms contribute some fraction of their total CB energy, depending on how they are intersected by the tessellation cells of the three repatoms by which they are defined. Element C, which has two-thirds of its area intersected by the tessellation cells of local repatoms, will contribute two-thirds of the energy it contains according to the CB rule. Similarly, since element D contacts only one local repatom, it will contribute only one third
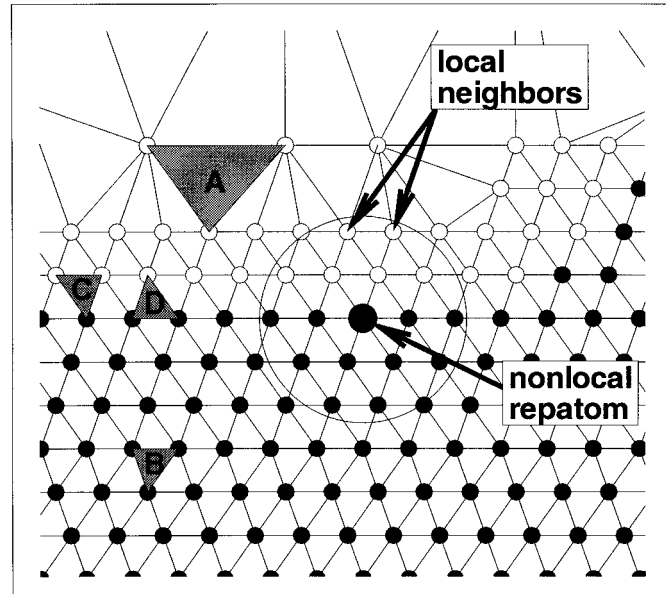
Figure 6. The atomistic/continuum transition region for the QC method. The gray elements do not contribute their full energy to the system because they are tied to interface atoms.

of its energy. This prescription, which follows naturally from eqn. (25), accounts for the fact that some of the energy in these elements is already accounted for in the energy of its nonlocal repatoms.

As in all attempts to couple a nonlocal atomistic region to a local continuum region found in the literature[5], a well-defined energy functional for the entire QC model will lead to spurious forces near the interface. These forces, dubbed "ghost-forces" in the QC literature, arise due to the fact that there is an inherent mismatch between the local (continuum) and nonlocal (atomistic) regions in the problem. In short, the finite range of interaction in the nonlocal region mean that the motion of repatoms in the local region will effect the energy of nonlocal repatoms, while the converse may not be true. This is again shown in Fig. 6, where one nonlocal repatom is shown enlarged and within a circle indicating the range of the EAM interactions. Because this nonlocal repatom sees local repatoms as neighbors, the motion of these local repatoms will directly affect its energy. On the other hand, the energy of the local neighbors depends only on the deformation in the elements adjacent to them, and therefore it is not affected by the highlighted nonlocal repatom. Upon differentiating eqn. (25), forces on repatoms in the vicinity of the interface will include a nonphysical contribution due to this asymmetry. Note that these "ghost forces" are a consequence of differentiating an approximate energy functional, and therefore they still are "real" forces that satisfy Newton's third law. The problem is that the mixed local/nonlocal energy functional of eqn. (25) is approximate, and the error in this approximation is most apparent at the interface. A consequence of this is that a perfect, undistorted crystal containing a local/nonlocal interface will be able to lower its energy below the ground state energy by rearranging the atoms in the vicinity of the interface. This is clearly a non-physical result.

In reference [8], a solution to the ghost forces was proposed whereby corrective forces were added as dead loads to the interface region. The assumption, in this case, was that the ghost forces would not change much during the minimization process. In this way, there is a
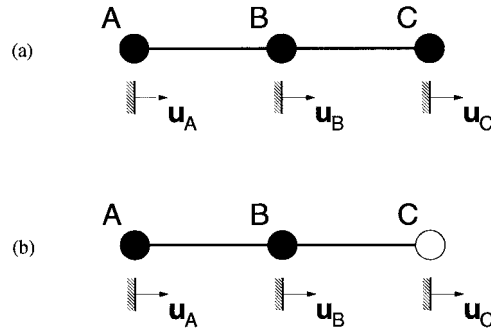
Figure 7. One-dimensional chains used to explain the ghost force correction procedure. Frame (a) shows a fully nonlocal chain, and frame (b) a chain containing two nonlocal atoms and one local atom.

well-defined contribution of the corrective forces to the total energy functional (since the dead loads are constant) and the minimization of the modified energy can proceed using standard conjugate gradient or Newton-Raphson techniques.

To clarify the ghost force correction procedure we consider the 1D chains of three atoms in Fig. 7. We start with a fully nonlocal chain (Fig. 7(a)). Assuming second-neighbor interactions the total energy of the chain is

$$E^{tot} = E_A^{NL}(u_A, u_B, u_C) + E_B^{NL}(u_A, u_B, u_C) + E_C^{NL}(u_A, u_B, u_C), \tag{28}$$

where E_A^{NL}, E_B^{NL} and E_C^{NL} are the energies of atoms A, B and C, respectively. The superscript "NL" indicates that the energies are computed nonlocally. Due to the second-neighbor interactions, the energy of each atom depends on the displacements of all other atoms. The forces on the atoms, f_A, f_B and f_C, follow by differentiation,

$$-f_A = \frac{\partial E^{tot}}{\partial u_A} = \frac{\partial E_A^{NL}}{\partial u_A} + \frac{\partial E_B^{NL}}{\partial u_A} + \frac{\partial E_C^{NL}}{\partial u_A}, \tag{29}$$

$$-f_B = \frac{\partial E^{tot}}{\partial u_B} = \frac{\partial E_A^{NL}}{\partial u_B} + \frac{\partial E_B^{NL}}{\partial u_B} + \frac{\partial E_C^{NL}}{\partial u_B}, \tag{30}$$

$$-f_C = \frac{\partial E^{tot}}{\partial u_C} = \frac{\partial E_A^{NL}}{\partial u_C} + \frac{\partial E_B^{NL}}{\partial u_C} + \frac{\partial E_C^{NL}}{\partial u_C}. \tag{31}$$

Here u_A, u_B and u_C are the displacements of atoms A, B and C along the chain direction. Now consider the case of the mixed local/nonlocal chain in Fig. 7(b). The chain contains two nonlocal atoms and one local atom. The total energy of the chain is

$$E^{tot} = E_A^{NL}(u_A, u_B, u_C) + E_B^{NL}(u_A, u_B, u_C) + E_C^L(F_{BC}). \tag{32}$$

The contributions of the nonlocal atoms A and B remain the same as in the fully nonlocal chain. Atom C is now local and its energy E_C^L depends on the deformation gradient F_{BC} in the element BC immediately adjacent to it. For the 1D case this deformation gradient is simply $F_{BC} = (u_C - u_B)/L_{BC}$, where L_{BC} is the length of element BC. The forces on the atoms are now,

$$-f_A = \frac{\partial E^{tot}}{\partial u_A} = \frac{\partial E_A^{NL}}{\partial u_A} + \frac{\partial E_B^{NL}}{\partial u_A}, \tag{33}$$

$$-f_B = \frac{\partial E^{tot}}{\partial u_B} = \frac{\partial E_A^{NL}}{\partial u_B} + \frac{\partial E_B^{NL}}{\partial u_B} + \frac{\partial E_C^{L}}{\partial F_{BC}}\frac{\partial F_{BC}}{\partial u_B}, \tag{34}$$

$$-f_C = \frac{\partial E^{tot}}{\partial u_C} = \frac{\partial E_A^{NL}}{\partial u_C} + \frac{\partial E_B^{NL}}{\partial u_C} + \frac{\partial E_C^{L}}{\partial F_{BC}}\frac{\partial F_{BC}}{\partial u_C}. \tag{35}$$

Our objective in applying the ghost-force correction is to ensure that the force on each atom is consistent with its status. This means that forces on nonlocal atoms near a local/nonlocal interface should be the same as those of atoms in a fully nonlocal formulation and forces on local atoms near the interface should be the same as those of atoms in a fully local formulation. Comparing the forces in mixed local/nonlocal chain to those computed earlier for the fully nonlocal chain, we see that this criterion is not satisfied for the nonlocal atoms. Relative to the fully nonlocal formulation, the force on atom A in the mixed chain is missing the third term and the force on atom B has an incorrect third term. Similarly the force on the local atom in the mixed formulation contains contributions from the nonlocal atoms which should not be there. To correct for this an auxiliary potential energy function $\tilde{\Phi}$ is defined for the mixed formulation where missing terms are added on as dead loads and extraneous terms are subtracted off,

$$\tilde{\Phi} = E^{tot} + \left(\frac{\partial E_C^{NL}}{\partial u_A}\right)u_A + \left(-\frac{\partial E_C^{L}}{\partial u_B} + \frac{\partial E_C^{NL}}{\partial u_B}\right)u_B + \left(-\frac{\partial E_A^{NL}}{\partial u_C} - \frac{\partial E_B^{NL}}{\partial u_C}\right)u_C. \tag{36}$$

For the general n-dimensional case an analogous expressions is defined,

$$\tilde{\Phi}(\boldsymbol{u}) = \Phi(\boldsymbol{u}) - \sum_{\alpha=1}^{N_{rep}}\boldsymbol{f}_\alpha^G \cdot \boldsymbol{u}_\alpha, \tag{37}$$

where $\boldsymbol{f}_\alpha^G$ are the ghost-force correction terms and $\boldsymbol{u}_\alpha$ the repatom displacements. As noted above, minimization is then applied to the auxiliary function $\tilde{\Phi}(\boldsymbol{u})$ to obtain the equilibrium configuration. If necessary, it is possible to iterate several times by recomputing the ghost-force corrections at the equilibrium configuration and re-minimizing, until self-consistency is achieved.

An alternative scheme to eliminate ghost forces is to abandon the requirement of a well-defined energy functional and instead drive the system to equilibrium by seeking a configuration for which the force on all the repatom is zero. By using this starting point, the forces need not be obtained strictly as derivatives of a single energy functional, and can instead be approximate expressions for a physically motivated set of forces. This is essentially the approach taken in the force-based formulation of the nonlocal QC, and has also been used by Shilkrot *et al.* [21] in a similar coupling of atomistic and continuum mechanics. Even in the absence of a well-defined energy functional, efficient numerical algorithms have been developed for finding the equilibrium configuration in a nonlinear force system such as the QC formulation.

3.5. EVOLVING MICROSTRUCTURE: AUTOMATIC MESH ADAPTION

The QC approaches outlined in the previous sections can only be successfully applied to general problems in crystalline deformation if it is possible to ensure that the fine structure in the deformation field will be captured. Without *a priori* knowledge of where the deformation

field will require fine-scale resolution, it is necessary that the method have a built-in, automatic way to adapt the finite element mesh through the addition or removal of repatoms.

To this end, the QC makes use of the finite element literature, where considerable attention has been given to adaptive meshing techniques for many years. Typically in finite element techniques, a scalar measure is defined to quantify the error introduced into the solution by the current density of nodes (or repatoms in the QC). Elements in which this error estimator is higher than some prescribed tolerance are targeted for adaption, while at the same time the error estimator can be used to remove unnecessary nodes from the model. The error estimator of Zienkiewicz and Zhu [22], originally posed in terms of errors in the stresses, is re-cast for the QC in terms of the deformation gradient. Specifically, we define the error estimator to be

$$\varepsilon_e = \left[\frac{1}{\Omega_e} \int_{\Omega_e} (\bar{F} - F_e) : (\bar{F} - F_e) d\Omega \right]^{1/2}, \tag{38}$$

where Ω_e is the volume of element e, F_e is the QC solution for the deformation gradient in element e, and $\bar{F}$ is the L_2-projection of the QC solution for F, given by

$$\bar{F} = SF_{avg}. \tag{39}$$

Here, S is the shape function array, and F_{avg} is the array of nodal values of the projected deformation gradient $\bar{F}$. Because the deformation gradients are constant within the linear elements used in the QC , the nodal values F_{avg} are simply computed by averaging the deformation gradients found in each element touching a given repatom. This is then interpolated throughout the elements using the shape functions, providing an estimate to the discretized field solution that would be obtained if higher order elements were used. The error, then, is defined as the difference between the actual solution and this estimate of the higher order solution. If this error is small, it implies that the higher order solution is well represented by the lower order elements in the region, and thus no refinement is required. The integral in equation eqn. (38) can be computed quickly and accurately using Gaussian quadrature. Elements for which the error ε_e is greater than some prescribed error tolerance are targeted for refinement. Refinement then proceeds by adding three new repatoms at the atomic sites closest to the mid-sides of the targeted elements. Notice that since repatoms must fall on actual atomic sites in the reference lattice, there is a natural lower limit to element size. If the nearest atomic sites to the mid-sides of the elements are the atoms at the element corners, the region is fully refined and no new repatoms can be added.

The same error estimator is used in the QC to remove unnecessary repatoms from the mesh. In this process, a repatom is temporarily removed from the mesh and the surrounding region is locally remeshed. If the all of the elements produced by this remeshing process have a value of the error estimator below the threshold, the repatom can be eliminated.

4. Extensions and enhancements

4.1. POLYCRYSTALS

Up to this point in this article, the focus has been on modeling a single crystal. The assumption of a single crystal was tacit in eqn. (1), which facilitates the location of any atom in the reference crystal.

To model polycrystals, the body can be divided into contiguous domains representing the grains. Each grain μ has associated with it a unique set of Bravais lattice vectors A_i^μ, $\{i =$
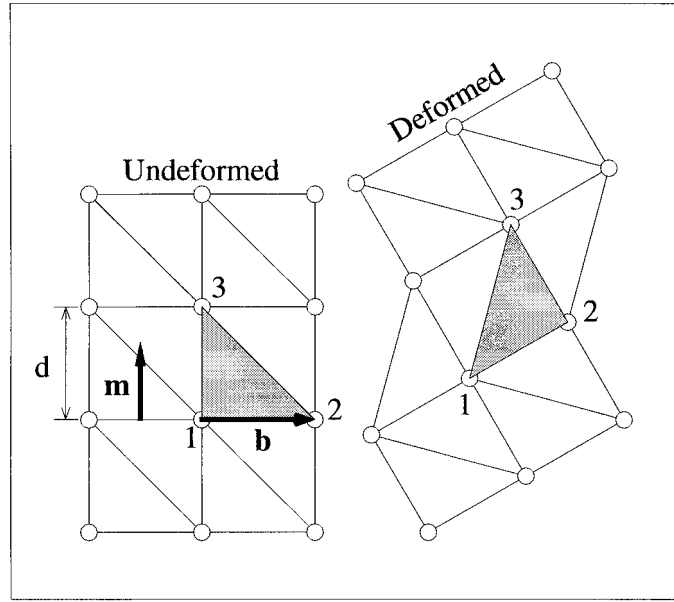
Figure 8. Idealized deformation involving perfect slip and rigid body translation and rotation of the lattice.

$1 \ldots 3\}$ and a unique reference atom X_0^{μ}. Repatoms are chosen in exactly the same manner as before, and a mesh is generated between the repatoms. Each element is assumed to reside entirely in one grain, so that in local regions the CB rule can be applied element-by-element. This implies that the grain boundaries in a polygranular QC simulation will necessarily follow a line of element edges (or surfaces in 3D).

In local regions of the QC simulation, the effect of modeling the body as polygranular is simply to introduce a non-uniform set of material properties, *i.e.*, each grain will have different elastic anisotropy and different crystal symmetry. Grain boundaries will not have any energy associated with them in the local regions. In nonlocal regions, the full grain boundary structure and energy can be accurately captured as long as the model is refined down to the atomic scale. In section 5, some examples of grain boundary simulations will be presented.

4.2. ELASTIC/PLASTIC DEFORMATION DECOMPOSITION

One disadvantage of the QC occurs when dislocations move over long distances in the initially perfect crystal. As a dislocation moves through a crystal, the QC must have an atomically-refined region around the dislocation core. This atomic-scale refinement will follow the core as it moves, leaving in its wake a band of high repatom density. Since the region through which the dislocation has swept is essentially perfect crystal, it is computationally inefficient to keep this high repatom density. To some degree, this problem can be eliminated by the implementation of mesh coarsening, as described briefly at the end of section 3.5, but the dislocation slip trace cannot be completely eliminated since there will always be elements on the slip plane that are sheared by an amount b/d (b is the Burgers vector, d is the interplanar spacing). Even though this b/d shear brings the crystal back into perfect registry, the large deformation in close proximity to elements with only relatively small elastic strains will trigger the nonlocality criterion and force full atomic scale refinement along the entire distance that the dislocation has moved.

This problem can be overcome by re-casting the nonlocality criterion and the automatic mesh adaption of sections 3.4.1 and 3.5 in terms of only the elastic part of the deformation. This is achieved by recognizing that the deformation gradient in each element can be decomposed into a plastic and elastic part as

$$F = F^e F^p. \tag{40}$$

For elements in fully refined regions (*i.e.* for which the element spans a single interplanar spacing in the crystal) there is a finite number of possible plastic deformation gradients F^p associated with lattice-restoring slip processes due to the passage of a dislocation. This is illustrated in Fig. 8, where the element joining repatoms 1, 2 and 3 undergoes the plastic deformation

$$F^p = I + \frac{b \otimes m}{d}, \tag{41}$$

where b is the Burgers vector, m is the slip plane normal and d is the interplanar spacing. Since this deformation restores perfect crystal registry, it does not contribute to the strain energy of the lattice, that is

$$\mathcal{E}(F^e) = \mathcal{E}(F^e F^p). \tag{42}$$

An algorithm has been developed whereby the deformation gradient is updated in elements that have been deformed by a lattice-restoring slip. Specifically, in the current deformed state of each element, there is a set of three deformed Bravais lattice vectors

$$a_j = F^e F^p A_j, \tag{43}$$

where A_j ($j = 1 \ldots 3$) are the three undeformed vectors and a_j are the deformed vectors. The algorithm attempts to make the deformed Bravais lattice in an element as close as possible (in a Euclidian norm sense) to those of the element's neighbors by applying the possible inverse plastic deformations, $(F^p)^{-1}$ of the type in eqn. (41). If it is found that one of these deformations will indeed improve the match between an element and its neighbors, the deformation gradient in the element is replace by

$$F^{new} = F(F^p)^{-1}. \tag{44}$$

Because both the nonlocality criterion and the mesh adaption error norm are defined in terms of the deformation gradients, comparing the updated F^{new} with that of the elements neighbors will not trigger nonlocality and simultaneously allow the mesh coarsening algorithm to remove the unnecessary repatoms in the region.

An example of the effect of this algorithm is shown in Fig. 9 for the region around a dislocation core in aluminum. On the left, the inefficient fine meshing of the slip plane is shown. On the right, the algorithm has left only the core region refined to the atomic scale. Note that the region of refinement around $(x, y) = (-110, 0)$ persists dues to the proximity of the nonlocal repatoms to a free surface, which is an issue different from the one being described here.
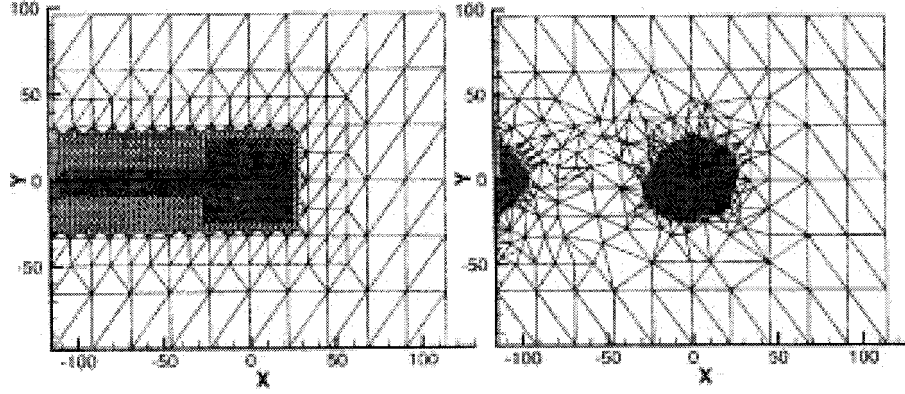
Figure 9. Removing the unnecessary slip plane adaption [23].

4.3. COMPLEX LATTICES

Much of the work with the QC has focused on materials with simple lattice structures. This means crystals that have only one atom attached to each Bravais lattice site defining the crystal periodicity. This permits the study of fcc and bcc metals, but precludes many important materials such as diamond cubic Si, hcp metals like Zr, and intermetallics like NiAl.

Several researchers [24, 25] have developed methods to extend the QC to the complex lattice. The main improvement which must be made is in the CB rule of section 3.2, which assumes that a macroscopically uniform deformation translates into a uniform deformation on the scale of the lattice. In fact, this is only true for simple lattices. In complex lattices, there are 3 additional degrees of freedom for each additional atom associated with the Bravais lattice site. In general, a complex lattice containing n atoms per Bravais site can always be described as n independent, interpenetrating Bravais lattices with the same lattice vectors but different origin positions. Thus, there is a vector $\boldsymbol{\delta}_i$ $(i = 2 \ldots n)$ defining the origin for each of the second through nth Bravais lattice relative to the origin of the first. When a uniform macroscopic deformation is applied, all the Bravais lattices undergo the same uniform deformation, but in addition the vectors $\boldsymbol{\delta}_i$ can change. To account for this correctly in the local QC, each calculation of the energy density must include a minimization on the internal degrees of freedom, $\boldsymbol{\delta}_i$, a process referred to as "shuffling". Thus,

$$\mathcal{E}(\boldsymbol{F}) = \min_{\boldsymbol{\delta}_i} \hat{\mathcal{E}}(\boldsymbol{F}, \boldsymbol{\delta}_i), \tag{45}$$

where $\hat{\mathcal{E}}(\boldsymbol{F}, \boldsymbol{\delta}_i)$ is the strain energy density of the lattice for arbitrary deformation and shuffle.

To date, the nonlocal QC has not been extended to complex lattices. The essence of the procedure is to define not repatoms, but representative Bravais sites with $3n$ degrees of freedom instead of the 3 degrees of freedom for the simple case. Initial tests suggest that the nonlocal QC could be extended to the complex lattice with reasonable efficiency and accuracy.
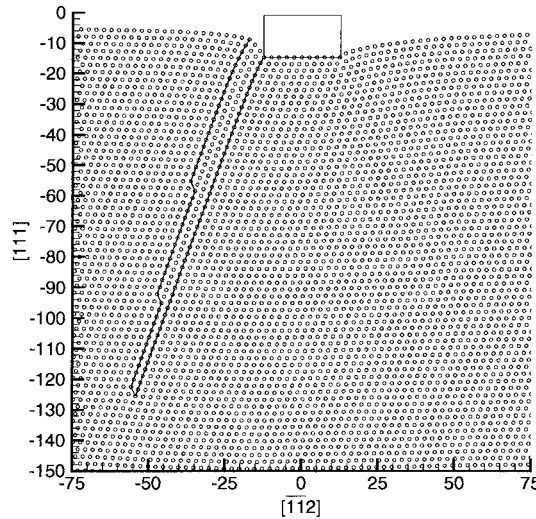
Figure 10. A deformation twin nucleated from the corner of a rectangular indenter pressed into the (111) surface of a single crystal of aluminum. The result was obtained from a QC simulation. Reprinted from [27], with permission.

5. Applications

In this section, we review some of the important results that have been obtained using the QC.

5.1. NANO-INDENTATION

One of the first deformation problems to be addressed using QC was nano-indentation [26, 27]. Nano-indentation experiments are typically carried out on the length scales for which the QC is designed: the experiments are too large to expect realistic system sizes and boundary conditions from a fully atomistic model, but the small numbers of dislocations involved and the atomic scale details of their nucleation require a fully atomistic treatment in some regions.

In [27], Tadmor *et al.* performed nano-indentation simulations in 2D using a rectangular and cylindrical indenter, with the focus on *incipient plasticity*. As the phrase suggests, this is a regime of crystal deformation just on the verge of full-scale plastic flow. Incipient plasticity involves the nucleation and motion of a few to tens of dislocations. The usefulness of the QC in studying this phenomena is manifest in the great detail with which one can analyze the deformation process, probing such issues as the stress, strain and slip distributions on the atomic scale. Tadmor *et al.* made several important observations, summarized in the following. First, careful analysis of the stresses and strains just prior to nucleation of the initial dislocations under the indenter suggested that a criterion based on critical shear stress correctly predicts dislocation nucleation for a rectangular indenter but not for a cylindrical one. Secondly, the work allowed for a thorough examination of the *mechanisms* of defect nucleation and motion. For example, Fig. 10 shows the formation of a microtwin during indentation by a rectangular indenter. In this orientation, the easy glide systems for the fcc crystal are constrained, allowing the more energetic twinning mechanism to occur. A similar twinning mechanism was observed by Picu [28] in bcc Mo, who also used the QC in his nano-indentation study.

In [29], the same QC simulations of a rectangular indenter from [30] were used to test a continuum-based dislocation nucleation criterion based on the Peierls-Nabarro (PN) model (as developed by Rice [30] for crack tip nucleation of dislocations). It was found that for a
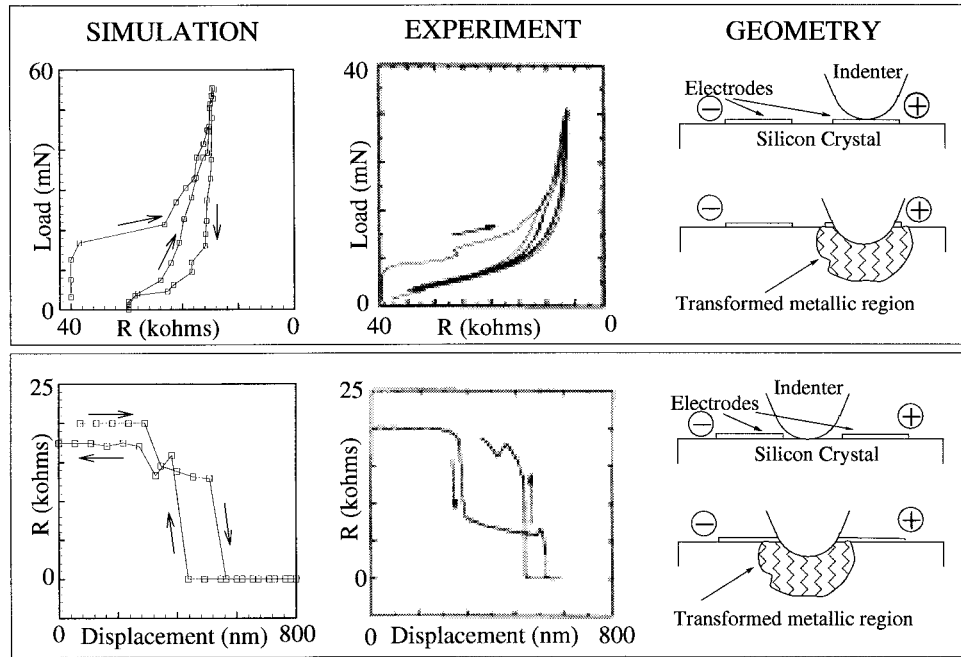
224

Figure 11. Comparison between QC simulation results and experimental results [31] for electrical resistance measured between two electrodes on a silicon surface subjected to indentation. Reprinted from [32], with permission.

rectangular indenter the PN model predicts a stress-based nucleation criterion in agreement with the simulation results. In both cases, dislocations are nucleated when the resolved shear stress at the tip of the indenter reaches a critical value which is independent of the width of the indenter. The theoretical analysis pointed out the importance of including ledge effects in order to obtain better quantitative agreement between analysis and simulation.

Indentation into diamond-cubic Si using a local QC implementation [32, 33] lead to the observation of stress-induced phase transformations beneath the indenter. It was found that during the indentation process, a roughly hemispherical region of transformed material composed of several different metallic phases, including β-tin, bct5 and bcc, forms beneath the indenter, growing with increasing load. During unloading, the region fragments forming a tendril-like structure of conducting material. The simulation reproduces the well-known hysteretic load-displacement curve of silicon nanoindentation, including the sudden discontinuity in the unloading curve which is often observed in experiment. In conjunction with a simple analytical model, the simulation was able to explain the experimentally observed change in electrical resistance measured between two electrodes on a silicon surface subjected to indentation. In these experiments the change in resistance between the electrodes is measured as an indenter is pressed either into one of the electrodes or between the two electrodes. A drop in resistance is observed with increasing indentation, a fact often cited as proof that transition to a metallic phase is occurring. Fig. 11 shows a comparison between the simulation results and experimental measurement for indentation load versus resistance and resistance versus indentation depth for the two loading scenarios (on or between the electrodes). The agreement is striking. The simulations were carried out using both the empirical SW potential for silicon

and a TB formulation for silicon due to Bernstein and Kaxiras [34]. The main conclusions of the analysis were found to be independent of the potential used.

A 3D nano-indentation by a frictionless spherical indenter into an fcc crystal was the focal point of a QC study by Knap and Ortiz [9]. In these calculations, the fully nonlocal, force-based QC formulation was used. The main goal of these indentation simulations was as a test case to study the error bounds and convergence of the QC, facilitated by several comparisons with fully atomistic simulations of the same process.

5.2. Crack-Tip Deformation

One class of applications to which the QC is particularly well-suited is the study of deformation mechanisms at the tip of atomically-sharp cracks. In these problems atomic resolution is required in a very small region at the tip of the crack, while the continuum boundary conditions of linear elastic fracture mechanics (LEFM) need to be applied in the far field. The QC approach is particularly suited to studying the initiation of deformation at the crack tip such as bond breaking leading to a brittle response or a ductile response through dislocation emission.

Miller *et al.* [35] used the QC to study the deformation at the tips of cracks in single crystal nickel. Two different orientations were tested, one where the crystal cleaved in brittle fashion as a result of the applied mode I loading, and the other where dislocations were emitted. Use of the QC ensured that the model boundaries were distant enough not to effect the observed mechanisms or the critical loads at which they appeared. Miller *et al.* used the QC results to test analytical criteria for crack deformation, such as the Griffith criterion for brittle fracture and the Rice [30] criterion, which is based on the PN model, for dislocation emission. It was found that while the Griffith criterion was quantitatively accurate for the brittle case, the Rice criterion was less so. The Rice criterion underpredicted the critical load in the ductile orientation by 45% and predicted a ductile response for the brittle orientation as well. The authors studied the source of the error of the Rice model and conclude that it is most likely tied to the PN model assumption that all nonlinearity is confined to a single plane, whereas in the simulation it is was clear that the nonlinearity is more widely distributed.

Pillai and Miller [36] extended this investigation of crack tips to cracks on bi-material interfaces. The goal of the QC simulations was to systematically vary the atomic interactions between crystals at a fully coherent, epitaxial interface and study the effect of the interactions on the fracture properties of the interface. The authors found that under certain conditions, it was not possible to predict the ductile or brittle behaviour of the interface from a simple Griffith picture of brittle fracture. This was due to the fact that some interfaces would behave in an initially ductile fashion, emitting dislocations and blunting the crack. However, this blunting also created ledges at the crack tip that exposed different atomic layers, away from the true atomic scale "interface," to high crack tip stresses. These planes could then act as brittle cleavage paths. In other words, brittle bi-material interface fracture not only arises due to the clean cleavage of the two materials along the atomically well-defined interface, but also may include fracture such that a few atomic layers of one material are left on the fracture surface of the other material. An initially ductile respond (*i.e.* dislocation emission from the crack tip) can serve to facilitate brittle fracture along cleavage planes away from the interface.

More recently Hai and Tadmor [37] used the QC to study deformation processes at the tip of cracks in single-crystal aluminum for a variety of loading modes and orientations. The authors were particularly interested in investigating whether deformation twinning (DT)

would occur under certain conditions. DT in aluminum was observed previously by Tadmor *et al.* [27] under the tip of a rectangular indenter, as discussed above and shown in Fig. 10. The observation of DT in aluminum was a surprising result since DT is uncommon in fcc metals in general and in aluminum, in particular, it was traditionally assumed not to occur. However, DT at the tips of cracks in aluminum has been observed experimentally *in situ* in TEM in two instances [38, 39]. The objective of the QC analysis was to reproduce the experimental results, if possible, and to clarify the conditions under which DT occurs. The QC results showed that the deformation mechanism at the crack tip strongly depend on the loading mode, crystallographic orientation and crack tip morphology. For the experimental orientations DT was observed in the simulation in agreement with experiment. For other orientations either DT, dislocation emission or, in one instance, the formation of an intrinsic-extrinsic fault were observed. The complex response behavior observed in the simulations led the authors to develop a theoretical model for the nucleation of deformation twins based on the PN model [40]. The model is similar in spirit to that of Rice [30] for dislocation emission and serves as an extension to it for DT. The main result of this analysis is that DT is controlled by an energetic parameter, named by the authors the *unstable twinning energy*, in analogy to Rice's unstable stacking energy, which plays a similar role for dislocation emission. The predictions of the analytical model are in good agreement with the QC simulation results.

5.3. Deformation and Fracture of Grain Boundaries

The extension of the QC to allow the modeling of polycrystals opened the door to a host of interesting questions regarding grain boundaries (GBs). As with the example of nano-indentation, questions surrounding deformation at GBs are well-suited to the QC methodology, which allows for full atomic resolution near the boundary but large enough system sizes to provide realistic boundary conditions.

A very simple example of a GB simulation with the QC was provided in [7], in which a stepped twin boundary was subjected to shear loading parallel to the boundary plane. The QC simulation revealed the mechanism by which the boundary migrated under load: the nucleation of a pair of Shockley partial dislocations that traveled out from the step and along the boundary plane.

In [8], nano-indentation was used as a source of dislocations to interact with a grain boundary. The interaction between $[\bar{1}10]$ dislocations and a $\Sigma = 7(2\bar{4}\bar{1})$ GB was examined, and the main result is shown in Fig. 12. In (a), the configuration just before nucleation of the first defect reveals the perfect GB structure. In (b), the first dislocation is nucleated, and it immediately absorbed by the GB, forming a step. Finally, the next dislocation, dissociated into partials, stands off from the GB, forming a pile-up due to elastic interaction with the first emitted defect. For this particular boundary, no transmission of slip to the neighboring grain occurred.

Miller *et al.* [35] studied the effects of an impinging crack on two different GBs in fcc Al. In the first case, shown in Fig. 13, the mode I loading of the crack initially leads to high stresses along the GB. These stresses lead to the nucleation of dislocations that travel into the bulk of the two grains. Another effect of the crack tip stresses is the migration of the boundary, which actually bows to meet the crack tip as shown in Fig. 13(c). Finally, the crack begins to advance, but is stopped and blunted by the GB.

In contrast to the GB of Fig. 13, the second orientation studied by Miller *et al.* shows the brittle response of Fig. 14. In this case, the orientation is such that slip on the {111} planes
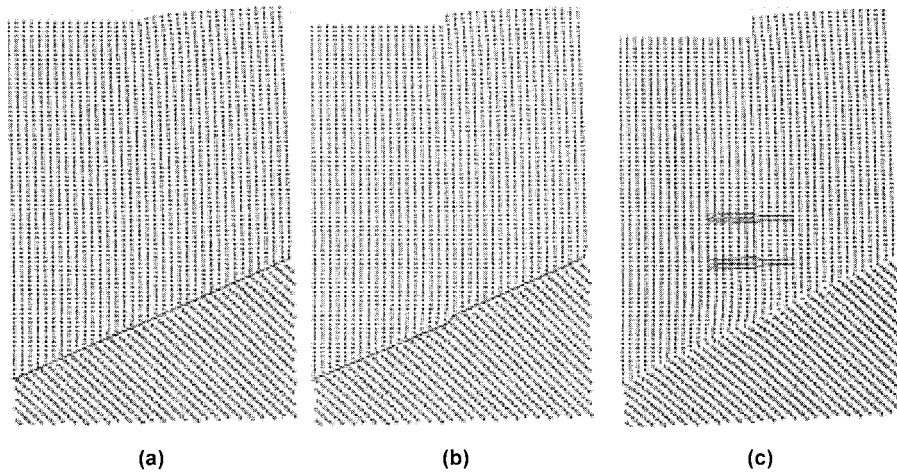
Figure 12. QC simulation of dislocations interacting with a grain boundary. Reprinted from [8], with permission.

is constrained, and the failure is by brittle cleavage. The GB itself serves as a path for rapid fracture. The results highlight the importance of grain boundary orientation and structure in fracture. Depending on the details of the GB, it may serve to either toughen or embrittle the polycrystal.

The GB-crack interactions of Miller *et al.* were a quasi-static, 2D simulation, but they were recently used as the starting point for a fully atomistic, 3D molecular dynamics study of the same GB-crack interactions by De Koning *et al.* [2, 41]. In these simulations, dynamic and 3D effects lead to dislocation loops forming at the crack tip and ultimately impinging on the GB. Through a systematic study of different boundary orientations, De Koning *et al.* observed varying degrees of slip transmission though the GB, and were able to develop a continuum model to predict the propensity for a specific GB to block dislocation transmission.

5.4. DISLOCATION INTERACTIONS

A key application of the 3D QC has been the study of the strength of dislocation junctions [26, 42, 43]. Rodney and Phillips [42] built QC simulations of dislocations lying in intersecting slip planes, and computed the critical stress required to break the dislocation junction. Fig. 15 shows the equilibrium configurations of one such junction at progressively larger levels of applied shear stress. In (a), we see the unstressed junction configuration. In (b) and (c), the junction stretches in response to the loading, and finally breaks apart as shown in (d). More recently, the interaction between dislocations and second-phase particles has been investigated in detail with the QC and compared with continuum predictions [44]. The main conclusion from this analysis is that provided that the continuum model includes key elements of the system, such as line-tension effects and the the presence of partial dislocations, the atomistic and continuum models yield the same picture for dislocation-obstacle interaction.

Mortensen *et al.* [45] used their own implementation of the QC named "ASAP" to study cross-slip of screw dislocations and jog mobility in copper. ASAP corresponds to a mixed local/nonlocal QC with some modifications making it easier to include QC as an add-on to standard lattice statics packages. In the cross-slip simulation, the nudged elastic band (NEB) method [46] was used in conjunction with ASAP to study the minimum energy path for the cross-slip of a [110]/2 screw dislocation. Use of ASAP translated to a savings of more
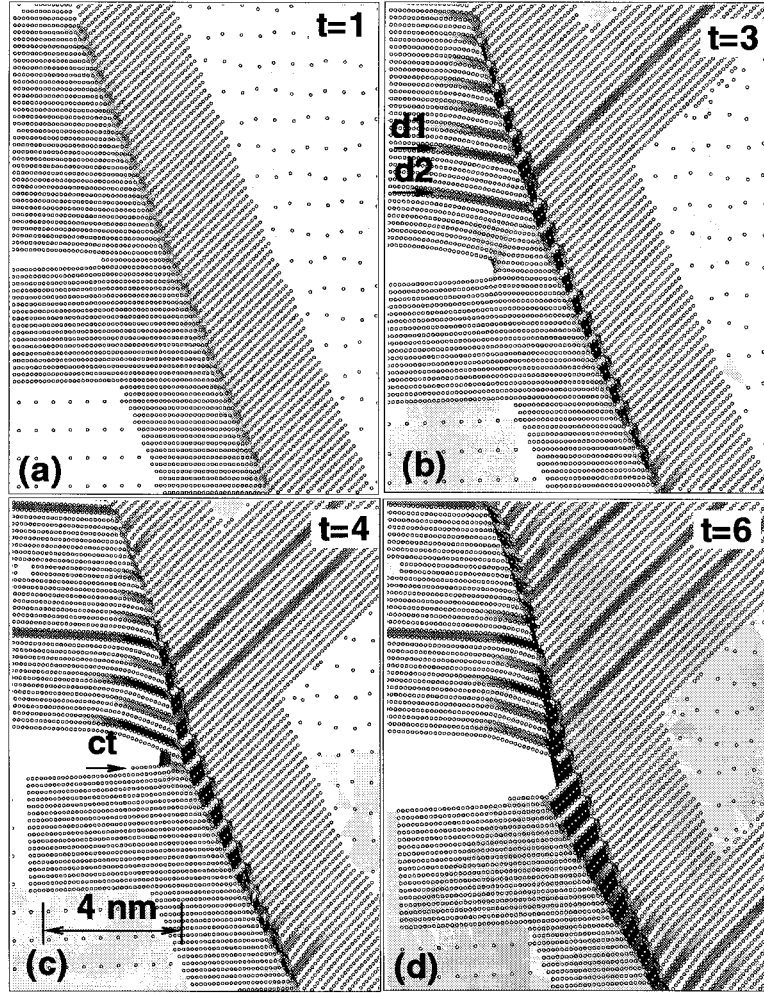
Figure 13. QC simulation of a crack impinging on a $\Sigma = 21(421)$ grain boundary. The time scale t indicates quasi-static load increments. $d1$ and $d2$ identify two typical dislocations being emitted from the grain boundary, while ct denotes the original location of the crack tip before crack advance. Reprinted from [35], with permission.

than a factor of 10 in the number of atoms needed for the analysis and in the computation time for a force calculation. For example, ASAP required 98,100 repatoms for the analysis compared with 1,152,000 atoms which would be required for a full atomistic simulation. The analysis showed that cross-slip occurs by a zipping and unzipping process, as seen in Fig. 16, in excellent agreement with earlier full atomistic simulations of Rasmussen *et al.* [47].

5.5. POLARIZATION SWITCHING IN FERROELECTRICS

Tadmor *et al.* [48] used the local QC formulation to study the response of ferroelectric lead-titanate (PbTiO$_3$) to electrical and mechanical loading. PbTiO$_3$ has a complex Bravais lattice structure and thus shuffling must be accounted for in the analysis. To this end, the complex lattice formulation of Tadmor *et al.* [24] was used. In order to correctly account for the constitutive response of a complex material like PbTiO$_3$ it is necessary to use accurate atomic description such as that of DFT. It is possible to directly incorporate a DFT engine into a local
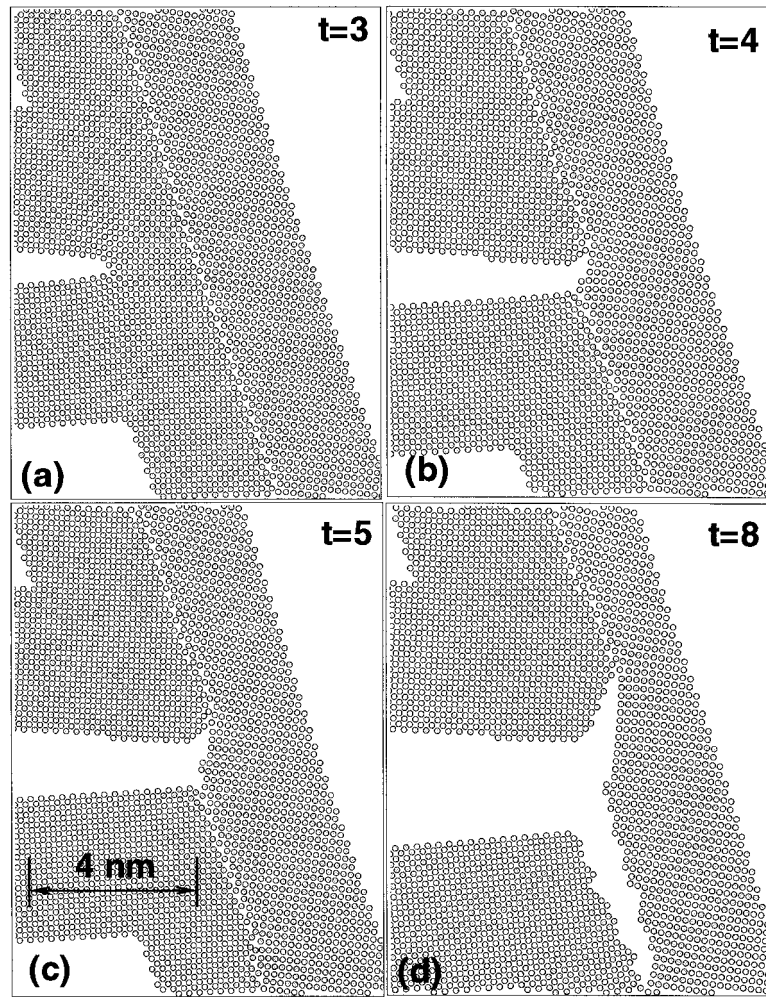
Figure 14. QC simulation of a crack impinging on a $\Sigma = 5(\bar{1}20)$ grain boundary. The time scale t indicates quasi-static load increments. Reprinted from [35], with permission.

QC formulation and this has been done before [49]. Unfortunately, due to the computational intensity of DFT calculations it is not presently possible to carry out large-scale computations with on-the-fly DFT constitutive calculations. As an alternative, Tadmor *et al.* [48] constructed an effective Hamiltonian for $PbTiO_3$ with coefficients fitted to a database of DFT calculations. This Hamiltonian is a nonlinear high-order expansion in finite strain, internal degrees of freedom and electric field. It contains the nonlinearity necessary for switching from the ground-state tetragonal phase of $PbTiO_3$ to the metastable rhombohedral and orthorhombic phases. The effective Hamiltonian was incorporated into the complex local QC formulation and was used to study hysteresis of single-crystal $PbTiO_3$ as a function of applied electric field and temperature and to analyze the microscopic mechanisms responsible for polarization switching. The model was also used to simulate a high-strain ferroelectric actuator proposed by Shu and Bhattacharya [50] and was able to reproduce the main qualitative features of the device. Fig. 17 shows a QC result for the device.
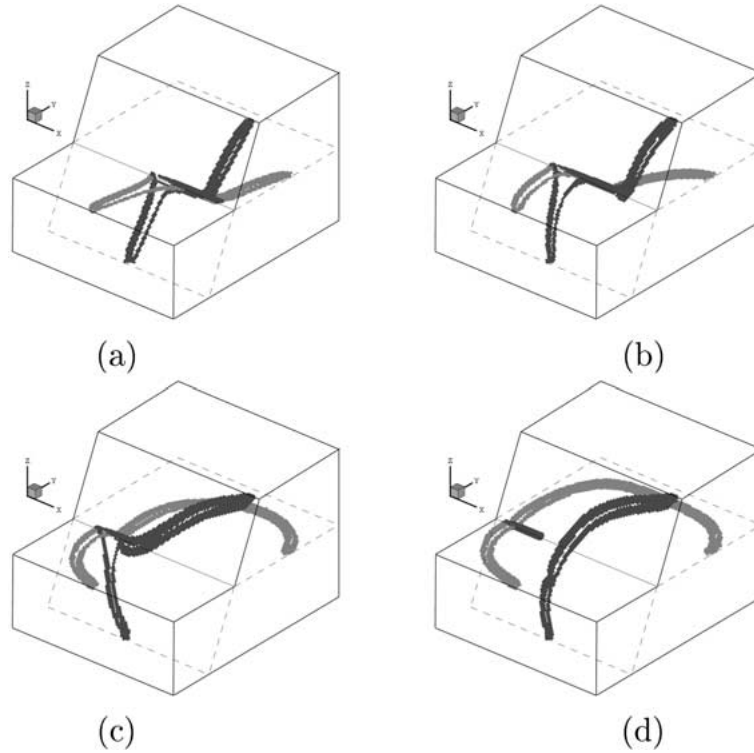
Figure 15. A 3D QC simulation of breaking a dislocation junction. (a)–(d) Equilibrium configurations with increasing level of applied shear stress. Only high energy atoms near the dislocations cores are shown. Reprinted from [42], with permission.

6. Current directions: Dynamics and finite temperatures

Up to this point, the development of the QC has focused on zero temperature static equilibrium problems. There are two key assumptions in this formulation. The first is zero temperature, which implies that the thermal vibration of the atoms about their lattice positions is not important. The second is *static equilibrium*, implying that we can neglect dynamic and inertial effects in the deformation of interest. A current direction in QC research is the development of algorithms that allow for both finite temperature and dynamic effects to be modeled in a QC framework without losing the essential philosophy of the QC approach: the systematic removal of a large fraction of the degrees of freedom and the explicit treatment of only a small subset of the atoms in the problem.

Formulating a dynamic, finite temperature QC (or "hot QC" as it is sometimes referred to) is indeed a significant challenge that would mark a tremendous step forward in our understanding of the links between atomistic and continuum modeling. To date, the approach has been to treat each of the two key assumptions individually. First, to consider a dynamic, zero temperature QC, and then to seek a QC formulation for which equilibrium configurations can be found at finite temperature. In the following, each of these extensions of the QC is examined in turn.
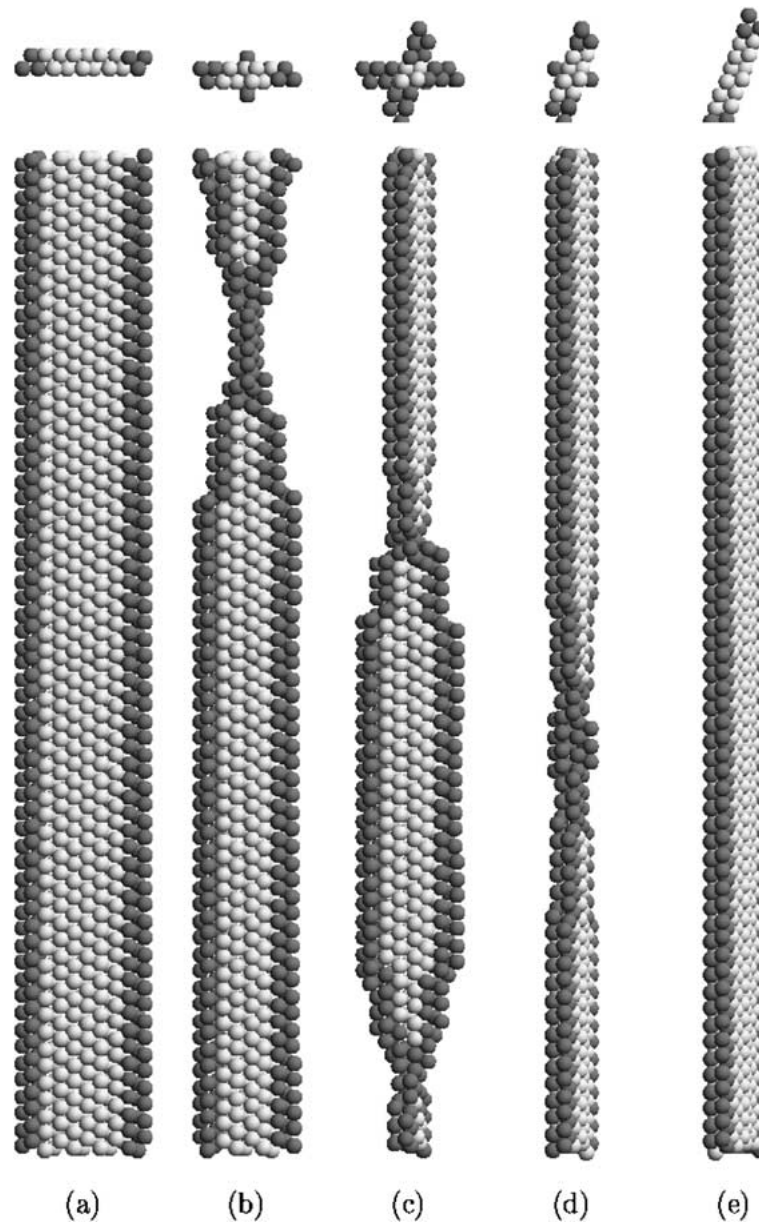
Figure 16. A 3D QC simulation of cross-slip of a dissociated [111]/2 screw dislocation. Frames (a) and (e) show the initial and final states of the process with the dislocation dissociated on the primary and cross-slip planes respectively. Frames (b),(c) and (d) show snapshots of the transition process, with (c) being the transition state (i.e., maximum energy state along the path). The top row corresponds to a view of the process along the dislocation line direction and the bottom row to a view normal to the primary slip plane. Reprinted from [45], with permission.

(a)   (b)
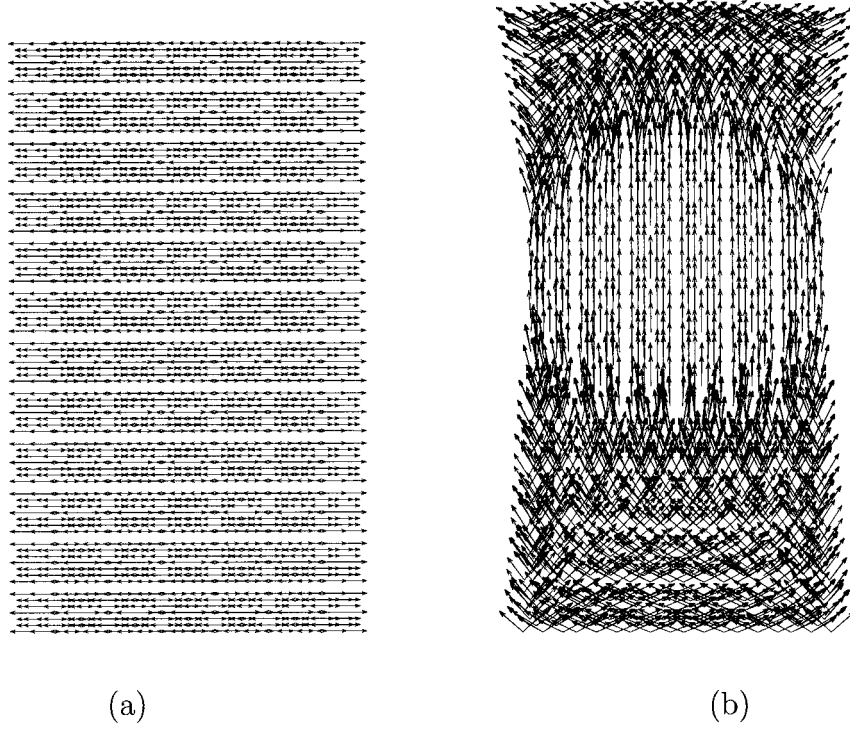
Figure 17. A local QC simulation of polarization switching in a slab of $PbTiO_3$ subjected to an electric field in the vertical direction. The arrows indicate the directions of polarization in individual finite elements. The simulation was 3D, the figure shows the results projected onto a single plane. Frame (a) shows the slab before application of the electric field. The directions of polarization are randomly distributed to the left and right resulting in an overall neutral material. Frame (b) shows the slab with an electric field of 120 MV/m applied to it in the vertical direction. The polarization in the central region has fully re-oriented in the vertical direction (the crystal has been "poled" there). The top and bottom of the slab are prevented by mechanical boundary conditions from fully re-orienting. Note the change in length of the slab in the vertical direction. This may be used as a basis for large-strain actuation. Note that the regular spacing between block of arrows in the figures is related to the tetragonal element shape in the 3D meshing and not to a physical property. Reprinted from [48], with permission from Elsevier Science.

6.1. ZERO TEMPERATURE DYNAMICS

It is straightforward in principle to modify the QC from a static to a dynamic simulation at zero temperature. The energy E^{tot} of eqn. (3), approximated by eqn. (25) for the mixed QC or eqn. (17) for the local QC, is simply the potential energy of the system for a given set of deformed atomic positions $X + u$. The kinetic energy of the system will be simply

$$KE = \sum_{\alpha=1}^{N_{rep}} \frac{1}{2} n_\alpha m \dot{u}_\alpha \cdot \dot{u}_\alpha, \qquad (46)$$

where the form of the expression is similar to that of a lumped-mass formulation in standard finite element techniques. The mass associated with each repatom is the weight n_α times the mass of a single atom, m. The velocities of any atoms not chosen as repatoms are simply the interpolated velocity field from the repatoms, as is the case for the displacements. Forces on the repatoms arise from the derivatives of the approximate potential energy, from which the acceleration of each repatom is found to be

$$n_\alpha m \dot{\boldsymbol{u}}_\alpha = \boldsymbol{f}_\alpha = -\frac{\partial E^{tot}}{\partial \boldsymbol{u}_\alpha}. \tag{47}$$

From these equations, a standard numerical scheme such as the Verlet algorithm can be used to evolve the repatoms through time.

The dynamic, zero temperature QC was implemented by Shenoy [51] and used to study nano-indentation and fracture processes. A key limitation to this approach is the non-physical impedance to phonon propagation due to the non-uniform mesh. In brief, the shortest wavelength phonon that can propagate through an element is equal to the characteristic length of the element. Thus, short wavelength phonons in the atomically-refined regions cannot be transmitted into the regions of lower repatom density and are reflected back. The result is a build-up of energy in the atomically refined region, which amounts to a localized, non-physical heating of the crystal.

Several authors have proposed boundary conditions between regions of full atomic detail and "continuum" regions of lower repatom density that serve to minimize the problem of phonon reflections and thus eliminate this problem. For example, Cai *et al.* [52] have recently proposed a method based on a linear Green's function description of interactions between atoms in the atomistic region and those in the continuum. Once a separate set of test simulations is performed to compute the response functions that characterize these interactions, an algorithm is devised such that the reflections from the atomistic/continuum boundary are minimized.

The method of Cai *et al.* [52], while providing excellent correction of the reflection problem, suffers from a high degree of computational complexity that may make it difficult to apply to general problems. More recently, E and Huang [53] have proposed a matching condition that is more approximate, but may be more amenable to implementation in the QC. In essence, the method is equivalent to the calculation of the Cai *et al.* [52] response functions only to the first few terms in a series expansion of the exact result. By choosing an optimal set of coefficients for the series, very good suppression of phonon reflection is achieved within a practical computational framework.

6.2. FINITE TEMPERATURE EQUILIBRIUM

To formulate the QC method at finite temperature, it is necessary to start from the partition function characterizing the equilibrium thermodynamics of the N atoms in the system

$$Z = \int e^{-\beta E^{tot}(\boldsymbol{u})} d\boldsymbol{u}, \tag{48}$$

where $\boldsymbol{u}$ in this equation implies the displacements of all the atoms, $\beta = (k_B T)^{-1}$, k_B is Boltzmann's constant, T is the temperature, and E^{tot} comes from eqn. (3). We then recognize that the QC philosophy is to formulate the problem based strictly on consideration of the *repatoms*. Thus, we can imagine partially computing the partition function by integrating over all atoms *not* explicitly chosen as repatoms, to obtain a renormalized partition function based only on the repatoms:

$$Z = \int e^{-\beta E^{tot}(\boldsymbol{u}^R, \boldsymbol{u}^C)} d\boldsymbol{u}^R d\boldsymbol{u}^C = \int e^{-\beta E^{eff}(\boldsymbol{u}^R, T)} d\boldsymbol{u}^R \tag{49}$$

where we have divided the atoms into repatoms (R) and all other atoms (C, the "constrained" atoms) and distinguish between the displacements of each subset of the atoms. We can use

this equation as the definition of an effective energy functional, E^{eff}, that depends only on the displacements of the repatoms and the temperature

$$e^{-\beta E^{eff}(\boldsymbol{u}^R, T)} = \int e^{-\beta E^{tot} d\boldsymbol{u}^C}. \tag{50}$$

Curtaloro and Ceder [54] have shown that this effective energy can be computed exactly only for very simple nearest neighbor atomic interactions. For realistic atomistic models, an approximation must be used to estimate E^{eff}. One such technique is that of Shenoy *et al.* [55], who assumed that a local harmonic approximation can be used in the computation of the integral in eqn. (50). Thus, it is assumed that the atoms, C, between the repatoms are harmonic oscillators about an equilibrium position dictated by the finite element interpolants of the repatom coordinates. Once this approximation is made, Shenoy *et al.* showed that the effective energy is the sum of the zero temperature QC energy and the entropic contribution that is effectively lost by treating the macroscopic, average variable u instead of the true microscopic displacements due to thermal vibrations of the constrained atoms. Because the local harmonic approximation is used, this entropic contribution can be computed and added to the zero temperature QC energy

$$E^{eff}(\boldsymbol{u}_R, T) = E^{tot,h}(\boldsymbol{u}_R) + 3k_B T \sum_{e=1}^{N_{element}} (n_e - 1) \frac{\hbar D^{\frac{1}{6}}(\boldsymbol{F}_e)}{k_B T}, \tag{51}$$

where the sum is over the elements, n_e is the number of atoms in element e, $\hbar$ is the Planck constant and D is the determinant of the dynamical matrix of an atom in an infinite crystal deformed according to the deformation gradient $\boldsymbol{F}_e$.

In the limit of a fully atomistic QC problem (where all atoms are chosen as repatoms), this formulation reduces to the local harmonic approximation applied, for example by [56, 57], to fully atomistic systems. Eqn. (51) can be used in Monte Carlo simulations of QC systems in finite temperature equilibrium, or used in the formation of a QC free energy by including the entropic contributions of the repatoms. However, the system is still not truly dynamic. This is because a key assumption in the derivation is that the system is is thermodynamic equilibrium, and it would be a violation of this assumption to simply use this effective energy in conjunction with the kinetic energy defined for zero-temperature dynamics in section 6.1. Further work in this direction is still needed to develop a rigorous theory for the dynamic, finite temperature coupling of atomistics and continuum mechanics in a QC framework.

7. Other multi-scale methods

In this section, we provide a brief review of a number of related works that are either closely related to the QC, are additional developments or applications of the QC, or represent alternative multiscale techniques that aim to address problems similar to those suited to the QC.

An interesting application of the local QC is presented by Gao and Klein [58, 59]. In this work, the idea of the QC to model atoms is extended to a QC model of more generalized "material particles". By considering a random array of material particles interacting according to a phenomenological force law, a QC-based constitutive law is created. The randomized nature of the material permits analytical progress to be made with the model, including a prediction of macroscopic elastic behaviour and conclusions about the limits of cohesion for the solid.

Finally, this formulation of the local QC was used to study dynamic fracture. Recently, this method has been re-visited and extended to probe more thoroughly the fracture behaviour of certain ideal classes of materials [60]. In particular, the problems of crack nucleation and propagation from a stress concentration, kinking of a mode II crack and buckling-driven delamination of thin films, were studied.

Van Vliet *et al.* [61] have implemented what is essentially the local QC, which they have called the "interatomic potential finite element method" or IPFEM. In this approach, the CB rule is used as the constitutive law, which is implemented as a user-subroutine in a commercial finite element software package. An important result of this work was the use of the IPFEM to test a criterion for the homogeneous nucleation of dislocations beneath an indented crystalline surface. The criterion, based on the criteria used to predict strain localization in plasticity [62, 63], uses the onset of instability in the nonlinear elastic (CB) constitutive law as a predictor for dislocation nucleation. The IPFEM results suggest that, in fact, the stability criterion does a good job of predicting defect nucleation.

Zhang *et al.* [64, 25] have used a local QC formulation, in which the extension to complex lattices described in 4.3 has been implemented, to study the behaviour of carbon nanotubes (CNT). The constitutive response of the the CNT is obtained by assuming a uniform deformation at each point on the surface of the tube and application of the complex lattice CB rule to the surface structure. The energetics of the deformation are computed using an empirical multi-body potential for carbon. Using this formulation the authors are able to obtain analytical solutions for various aspects of CNT deformation including an effective elastic modulus for the CNT and failure of the CNT through loss of stability.

An especially interesting application of the local QC was presented by Johnson *et al.* [65]. In this implementation, the underlying atomistic constitutive model for the CB rule was the TB method. The key advantage here is that the TB atomistic framework allows for the extraction of *electronic properties*, and more importantly the effect of strain on these properties. The researchers studied the effects of residual fabrication stresses and strains on semiconductor islands designed to behave as quantum dots. As in the IPFEM method described earlier, the local QC approach was implemented as a user-routine in a commercial finite element package, making available the sophisticated pre- and post- processing capabilities that such packages typically provide.

Currently, there are several researchers developing methods whereby an atomistic region is directly coupled to a continuum region. These methods are similar to the QC in their goals, but accomplish the task using a different approach. The most notable difference between the QC and the methods to be described here is the adaptability of the QC. The mesh adaption and nonlocality criterion of the QC allows the region of full, nonlocal atomic-scale resolution to evolve as dictated by the deformation. We will refer to methods that lack this adaptability as "coupled methods" to highlight the clear interface between the atomistic and continuum regions. Also, a recent review of several of these methods was written by Miller [17], and may be of interest to the reader of the present article.

One early coupled method is the FEAt model of [19, 66], which focused largely on the question of atomic scale fracture processes. In this approach, a non-linear elastic continuum is interfaced to an atomistic region using a nonlocal continuum as a transition. The method is limited to 2D, but has been used both for static and dynamic simulations. The careful treatment of the continuum and interface allowed for reasonably accurate calculation of critical energy release rates for fracture and crack tip blunting, allowing for a systematic comparison between
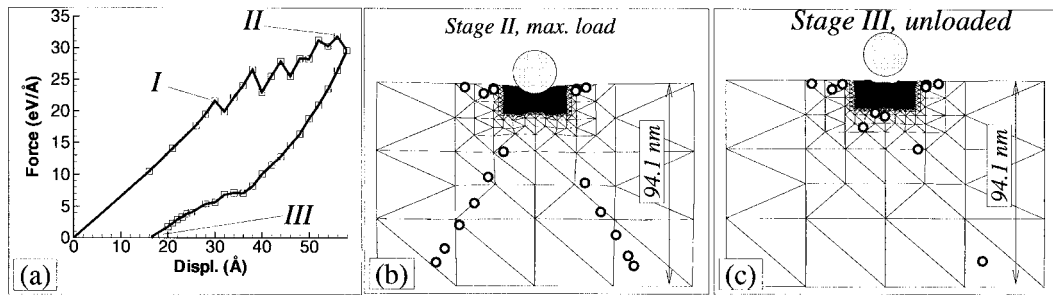
Figure 18. a CADD simulation of indentation by a spherical indenter. The load-displacement curve is shown in (a), while the deformed mesh and locations of the discrete dislocations are shown at maximum load in (b) and after unloading in (c).

the atomistic simulations and continuum-based criteria predicting brittle vs. ductile response [67].

The coupled method of Insepov *et al.* [68, 69] has been used to study the effects of impact by atomic clusters on crystal surfaces. It is a dynamic approach where an ensemble averaging technique is used to pass thermal and deformation information from the atomistic region to a surrounding FE mesh, preventing non-physical shock wave reflections from tainting the details of crater formation at the surface of the atomistic region.

Fracture was the initial focus of the *coupling of length scales* (CLS) method of [18, 70, 71], who have since taken advantage of powerful parallel computing to model fully three-dimensional problems of MEMS resonators [72, 73]. An example of the 3D resonator simulation is shown in Figures 1 and 4 of reference [72], which was used to study the dynamic response of the structure and its nano-scale contributions to dissipation. This development is significant, in that it represents a simulation of an entire engineered device, in contrast to the simulation of basic deformation phenomena typically investigated. In the original 2D version of the CLS technique, further progress in coupling methods was made by embedding a quantum-mechanically-based TB region inside the empirical atomistic region.

The more recent developments by Rudd and Broughton [74] recognize that the continuum-based origins of the FE method lead to difficulties in a smooth transition from the atomistic to the continuum. Thus, they have reformulated the continuum region using a method called coarse-grain molecular dynamics (CGMD), in which the degree-of-freedom reduction is developed as a more natural extension of the underlying discrete molecular dynamics. The CGMD method provides a replacement for the FE mesh typically used outside the atomistic region in coupled methods. Currently, the CGMD results have been limited to validation problems that demonstrate the capabilities of the method, but these initial results are encouraging and additional applications are an area of active research.

Another recent development has been to recognize that the continuum region can be augmented to expand the range of problems accessible to these methods. Specifically, the continuum region can be allowed to support dislocations as continuum defects. Such a development is important for problems involving dislocation motion in materials with relatively low lattice resistance, in which the defects can travel long distances and their influence on subsequent processes in the atomistic region is essentially only through their elastic fields. A coupled method, including algorithms to pass defects between that atomistic and continuum regions has been developed by Shilkrot *et al.* [20] and dubbed the *coupled atomistics and discrete dislocation* (CADD) method. In this approach, the continuum dislocations are modeled

via a superposition of the analytic solutions for dislocations in an infinite linear elastic solid, and then a linear elastic FE mesh is used to solve a complementary problem that corrects for the appropriate boundary conditions of the desired model geometry.

In Fig. 18, this method is used to model a 2D "spherical" nano-indentation. In (a), the load-displacement curve is shown and indicates the point of the first dislocation nucleation (*I*), maximum load (*II*) and unloaded (*III*). Dislocations are nucleated below the indenter in the atomistic region, and travel to the locations shown in (b) where they pile up against the constrained lower surface of the region. In (c), many dislocations remain in the film after unloading. CADD is well-suited to problems like this one when compared to the other coupled methods or the QC, which would require full atomic resolution wherever the CADD discrete dislocations are present.

8. Summary

This review has summarized the progress to date on the QC method, one of several current approaches to multiscale modeling of deformation processes. The QC method has been developed, extended and modified by a number of researchers over the course of the past seven years. During this time, the QC has served as both a key vehicle for our understanding of the nature of atomistic-continuum coupling and a practical tool for investigating problems requiring both an atomistic and continuum perspective.

Applications of the QC have included studies of nano-indentation, fracture, grain boundaries, dislocations and phase transformations. These applications are examples where neither atomistic simulation nor continuum mechanics alone were appropriate, whereas the QC was able to effectively combine the advantages of both modeling regimes. Examples provided in section 5 have demonstrated that the QC has become a truly predictive tool, allowing for the direct rationalization of experimentally observed materials phenomena.

Currently, the most important direction for the QC method is a complete dynamic theory of the QC at finite temperature. To this end, progress has been made in pieces; the QC has been extended to either zero temperature dynamics or finite temperature equilibrium formulations. The real challenge is to develop a computationally viable technique to approximate dynamic effects at temperature while staying true to the goal of substantial reduction in the total number of degrees of freedom in the problem.

Endnotes

[1]We omit, for now, a discussion of complex lattice with more than one atom at each Bravais lattice site. This topic is discussed in Section 4.3.

[2]The term "local" refers to the fact that use of the CB rule implies that the energy at each point in the continuum will only be a function of the deformation at that point and not on its surroundings.

[3]A simple lattice structure is one for which there is only one atom at each Bravais lattice site. In a complex lattice with two or more atoms per site, the Cauchy-Born rule must be generalized to permit shuffling of the off-site atoms. See section 4.3 for more details.

[4]A freely available version of this code, written in Fortran 90, may be downloaded from www.qcmethod.com.

238

[5]See [17] for a review of other types of coupled atomistic/continuum techniques, including [18, 19, 20].

References

1. Tadmor, E.B., Ortiz, M. and Phillips, R., Phil. Mag. A, 73 (1996) 1529.
2. de Koning, M., Miller, R., Bulatov, V.V. and Abraham, F.F., Phil. Mag. A, 82 (2002) 2511.
3. Ortiz, M., Cuitino, A.M., Knap, J. and Koslowski, M., MRS Bulletin, 26 (2001) 216.
4. Ortiz, M. and Phillips, R., Adv. Appl. Mech., 36 (1999) 1.
5. Rodney, D., Mixed atomistic/continuum methods: Static and dynamic quasicontinuum methods. In A. Finel, D. Maziere, and M. Veron, editors, Proceedings of the NATO Conference "Thermodynamics, Microstructures and Plasticity". Kluwer, Dortrecht, 2003. To appear.
6. Tadmor, E.B., Phillips, R. and Ortiz, M., Langmuir, 12 (1996) 4529.
7. Shenoy, V.B., Miller, R., Tadmor, E.B., Phillips, R. and Ortiz, M., Phys. Rev. Lett., 80 (1998) 742.
8. Shenoy, V.B., Miller, R., Tadmor, E.B., Rodney, D., Phillips, R. and Ortiz, M., J. Mech. Phys. Sol., 47 (1998) 611.
9. Knap, J. and Ortiz, M., J. Mech. Phys. Sol., 49 (2001) 1899.
10. Carlsson, A.E., Solid State Physics, 43 (1990) 1.
11. Daw, M.S. and Baskes, M.I., Phys. Rev. B, 29 (1984) 6443.
12. Norskøv, J.K. and Lang, N.D., Phys. Rev. B, 21 (1980) 2131.
13. Stillinger, F.H. and Weber, T.A., Phys. Rev. B, 31 (1985) 5262.
14. Zienkiewicz, O.C., *The Finite Element Method*, volume 1–2. McGraw-Hill, London, 4th edition (1991).
15. Ericksen, J.L., In M. Gurtin (Ed.), *Phase Transformations and Material Instabilities in Solids*, pp. 61—77. Academic Press, New York, 1984.
16. Okabe, A., *Spatial Tessellations: Concepts and Applications of Voronoi Diagrams*. Wiley and Sons, Chichester, England (1992).
17. Miller, R.E., *J. Multiscale Comput. Engin.*, 1 (2003) 57.
18. Rudd, R.E. and Broughton, J.Q., Phys. Stat Solidi B, 217 (2000) 251.
19. Kohlhoff, S., Gumbsch, P. and Fischmeister, H.F., Phil. Mag. A, 64 (1991) 851.
20. Shilkrot, L.E., Miller, R.E. and Curtin, W.A., Phys. Rev. Lett., 89 (2002) 025501–1.
21. Shilkrot, L.E., Miller, R.E. and Curtin, W.A., submitted to Acta Mat., 2003.
22. Zienkiewicz, O.C. and Zhu, J.Z., Int. J. Num. Meth. Engng., 24 (1987) 337.
23. Rodney, D. and Miller, R., unpublished, 1998.
24. Tadmor, E.B., Smith, G.S., Bernstein, N. and Kaxiras, E., Phys. Rev. B, 59 (1999) 235.
25. Zhang, P., Huang, Z., Geubelle, P.H., Klein, P.A. and Hwang, K.C., Int. J. Sol. and Struc., 39 (2002) 3893.
26. Phillips, R., Rodney, D., Shenoy, V., Tadmor, E.B. and Ortiz, M., Modeling Simul. Mater. Sci. Eng., 7 (1999) 769.
27. Tadmor, E.B., Miller, R., Phillips, R. and Ortiz, M., J. Mater. Res., 14 (1999) 2233.
28. Picu, P.C., J. Computer-Aided Materials Design, 7 (2000) 77.
29. Shenoy, V.B., Phillips, R. and Tadmor, E.B., J. Mech. Phys. Sol., 48 (2000) 649.
30. Rice, J.R., J. Mech. Phys. Sol., 40 (1992) 239.
31. Pharr, G.M., Oliver, W.C., Cook, R.F., Kirchner, P.D., Kroll, M.C., Dinger, T.R. and Clarke, D.R., J. Mater. Res., 7 (1992) 961.
32. Smith, G.S., Tadmor, E.B. and Kaxiras, E., Phys. Rev. Lett., 84 (2000) 1260.
33. Smith, G.S., Tadmor, E.B., Bernstein, N. and Kaxiras, E., Acta Mat., 49 (2001) 4089.
34. Bernstein, N. and Kaxiras, E., Phys. Rev. B, 56 (1997) 10488.
35. Miller, R., Tadmor, E.B., Phillips, R. and Ortiz, M., Modeling Simul. Mater. Sci. Eng., 6 (1998) 607.
36. Pillai, A.R. and Miller, R.E., Mat. Res. Soc. Symp. Proc., 653 (2001) Z2.9.1.
37. Hai, S. and Tadmor, E.B., Acta Mat., 51 (2003) 117.
38. Pond, R.C. and Garcia-Garcia, L.M.F., Inst. Phys. Conf. Ser., 61 (1981) 495.
39. Chen, Q., Huang, Y., Qiao, L. and Chu, W., Sci. China (Series E), 42 (1999) 1.
40. Tadmor, E.B. and Hai, S., J. Mech. Phys. Sol., 51 (2003) 765.
41. de Koning, M., Miller, R., Bulatov, V.V. and Abraham, F., Mat. Res. Soc. Symp. Proc., 677 (2001) AA1.5.1.
42. Rodney, D. and Phillips, R., Phys. Rev. Lett., 82 (1999) 1704.

43. Shin, C.S., Fivel, M.C., Rodney, D., Phillips, R., Shenoy, V.B. and Dupuy, L., Journal de Physique IV, 11 (2001) 19.
44. Hardikar, K., Shenoy, V. and Phillips, R., J. Mech. Phys. Sol., 49 (2001) 1951.
45. Mortensen, J.J., Schiøtz, J. and Jacobsen, K.W., Challenges Mol. Simul., 4 (2002) 119.
46. Henkelman, G., Uberuaga, B.P. and Jónsson, H., J. Chem. Phys., 113 (2000) 9901.
47. Rasmussen, T., Jacobsen, K.W., Leffers, T., Pedersen, O.B., Srinivasan, S.G. and Jónsson, H., Phys. Rev. Lett., 79 (1997) 3676.
48. Tadmor, E.B., Waghmare, U.V., Smith, G.S. and Kaxiras, E., Acta Mat., 50 (2002) 2989.
49. Tadmor, E.B. and Kaxiras, E., unpublished, 1997.
50. Shu, Y.C. and Bhattacharya, K., Phil. Mag. B, 81 (2001) 2021.
51. Shenoy, V., Shenoy, V. and Phillips, R., Mat. Res. Soc. Symp. Proc., 538 (1999) 465.
52. Cai, W., de Koning, M., Bulatov, V.V. and Yip, S., Phys. Rev. Lett., 85 (2000) 321.
53. Weinan, E. and Huang, Z., Phys. Rev. Lett., 87 (2001) 135501–1.
54. Curtaloro, S. and Ceder, G., Phys. Rev. Lett., 88 (2002) 255504.
55. Shenoy, V., Shenoy, V. and Phillips, R., Mat. Res. Soc. Symp. Proc., 538 (1999) 465.
56. LeSar, R., Najafabadi, R. and Srolovitz, D.J., Phys. Rev. Lett., 63 (1989) 624.
57. Foiles, S.M., Phys. Rev. B, 49 (1994) 14930.
58. Gao, H. and Klein, P., J. Mech. Phys. Sol., 46 (1998) 187.
59. Klein, P. and Gao, H., Engng. Fracture Mech., 61 (1998) 21.
60. Zhang, P., Klein, P.A., Huang, Y., Gao, H. and Wu, P.D., Computer Modeling in Engineering and Sciences, 3 2002) 263.
61. Van Vliet, K.J., Li, J., Zhu, T., Yip, S. and Suresh, S., Phys. Rev. B, 67 (2003) 104105.
62. Hill, R., J. Mech. Phys. Sol., 10 (1962) 1.
63. Rudnicki, J.W. and Rice, J.R., J. Mech. Phys. Sol., 23 (1975) 371.
64. Zhang, P., Huang, Y., Gao, H. and Hwang, K.C., J. Appl. Mech., 69 (2002) 454.
65. Johnson, H.T., Phillips, R. and Freund, L.B., Mat. Res. Soc. Symp. Proc., 538 (1999) 479.
66. Gumbsch, P., J. Mater. Res., 10 (1995) 2897.
67. Gumbsch, P. and Beltz, G.E., Modeling Simul. Mater. Sci. Eng., 3 (1995) 597.
68. Insepov, Z., Sosnowski, M. and Yamada, I., Nuclear Instruments and Methods in Physics Research B, 127 (1997) 269.
69. Insepov, Z., Manory, R., Matsuo, J. and Yamada, I., Phys. Rev. B, 61 (2000) 8744.
70. Broughton, J.Q., Abraham, F.F., Bernstein, N. and Kaxiras, E., Phys. Rev. B, 60 (1999) 2391.
71. Abraham, F.F., Broughton, J.Q., Bernstein, N. and Kaxiras, E., Comput. Phys., 12 (1998) 538.
72. Rudd, R.E. and Broughton, J.Q., J. Model. Sim. Microsys., 1 (1999) 29.
73. Rudd, R.E., Mat. Res. Soc. Symp. Proc., 677 (2001) AA1.6.1.
74. Rudd, R.E. and Broughton, J.Q., Phys. Rev. B, 58 (1998) R5893.